COIL MISALIGNMENT COMPENSATION TECHNIQUES FOR WIRELESS POWER TRANSFER LINKS IN BIOMEDICAL IMPLANTS

BY FANPENG KONG

A thesis submitted to the

Graduate School—New Brunswick

Rutgers, The State University of New Jersey

in partial fulfillment of the requirements

for the degree of

Master of Science

Graduate Program in Electrical and Computer Engineering

Written under the direction of

Professor Laleh Najafizadeh

and approved by

_____

_____

_____

New Brunswick, New Jersey

October, 2015

ABSTRACT OF THE THESIS

Coil Misalignment Compensation Techniques for Wireless Power Transfer Links in Biomedical Implants

by Fanpeng Kong

Thesis Director: Professor Laleh Najafizadeh

Wireless power Transfer (WPT) technique, based on inductive links, has been admitted as a promising solution for powering biomedical implants. Ensuring a stable power delivery via inductive links in implants under all conditions, however, has been a challenging design problem. One of the issues that negatively impacts the performance of wireless power transfer (WPT) links in implants, is the misalignment in the position of the transmitter and receiver coils, which could naturally occur as a result of body movement or changes in the biological environment. An immediate effect of coil misalignment is the change in coupling factor, resulting in the reduction of the power delivered to the load at the receiver side.

In this work, we present a design concept that could be employed on the transmitter side to mitigate this effect while keeping the driver to work at its optimum operating condition. Specifically, we will demonstrate, analytically and through simulations, that tuning the shunt capacitor and the supply voltage at the transmitter side could be

a promising approach for compensating the performance degradation induced by coil misalignment in WPT links.

Acknowledgements

I would like to express my sincere gratitude towards a number of individuals whose support, help and love have led me to reach this successful destination.

Firstly, I would like to thank my supervisor Dr. Laleh Najafizadeh for her patience guidance and encouragement. Her help and advice opened my vision and led me to reach several achievements during my journey in Rutgers University. The work cannot be finished without her insightful comments. My sincere gratitude will go to her again.

I would like to give my thank to my parents for their endless support and love. No matter what things happened, they always encouraged me to live strongly and face the difficulties positively. They gave me all they have to support me to pursue my dream and never asked for the return. My thank will also express to my beloved soul mate, Xinru, for her understanding and never-ending support. Her love has been the source of my motivation and strength.

Last but no the least, my thank will go to my friends for their help in my life. Also, I would like to thank my lab colleagues, Li Zhu and Yi Huang who are also my elder brothers for encouraging and helping me during my time in Rutgers University.

This work was supported in part by the National Science Foundation (NSF) under grant 1408202, and by a fellowship from the ECE Department at Rutgers University.

Table of Contents

List of Figures

Chapter 1

Introduction

The interest in biomedical implants has been gaining momentum since they have found applications in various domains such as: pacemakers [8] (to treat irregular hear beat), cochlear prostheses [9] (assist the deaf people with hearing) and multichannel neural recording systems [10] (for continuous monitoring of internal biosignal, namely, neural activities). Finding the optimum technique for delivering enough power to these biomedical implants has been a subject of several investigations [11] [12]. Conventionally, batteries are used to deliver the power, however, this approach offers several limitations. For example, the size, limited storage capacity and the number of recharge cycles render batteries as a non-ideal solution for powering biomedical implants as they need to be replaced via surgery [13]. Wireless power transfer is an alternative solution, which offers an attractive power delivery scheme for biomedical implants by limiting the need for battery replacement.

One of the popular techniques used for the realization of the wireless power transfer (WPT) scheme is inductive coupling [13]. The basic structure of this technique requires two inductors, one (primary coil) which is placed externally as the transmitter and another (secondary coil) which is placed inside the body at a short distance from the primary coil as the receiver. The power transfer capability of this system is highly depended on the coupling factor between the two coils [11]. However, the coils in biomedical implants for power transfer can be misaligned due to the movement of body,

which decreases the coupling factor and adversely affects the WPT to implants. This will deviate the driver of primary coil (class E power amplifier generally) from operating at its optimum working condition. The power delivered to the load is also changed due to the variance of the coupling factor. An 'ideal' approach to address the misalignment issue in WPT system of biomedical implants is to sense the changes induced by the misalignment and automatically self-reconfigure to compensate the negative effect of misalignment.

1.1 Motivation and research objectives

As one of the key factors which negatively affects the WPT system, the misalignment issue needs to be addressed. Recently, different compensation methods have been proposed. In [4], the working frequency of the system was suggested to be altered, which in turn changes the power transfer efficiency via the inductive links [5]. In [3] the drain inductor is tuned to mitigate the misalignment negative effect, but this approach requires an additional block to change the inductor. The goal of this work is to develop a new compensation concept to mitigate the misalignment issue without the disadvantages in [4] [3].

The research motivation is described as above and the research objectives of this Thesis is illustrated as follows. To eliminate the problems induced by the batteries in biomedical implants, a resonance-based inductively coupled links needs to be developed. An analytical study on misalignment needs to be performed to show its effect on the inductive links. The misalignment induced issue on the class E power amplifier and the power delivered to the load should be analyzed to identify the specific problems. After acknowledging the problems, a design method needs to be proposed for solving them.

1.2 Organization of the Thesis

In chapter 2, the theory behind the wireless power transfer technique is introduced in detail. The basic structure of wireless power transfer is also illustrated. The technique is classified into three categories based on the power transfer distance namely, near, mid and far field wireless power transfer.

In Chapter 3, different scenarios of the coil misalignment are discussed. To analyze these situations, the analytical method for coil misalignment are also presented in this chapter.

In Chapter 4, the existing work regrading the coil misalignment compensation methods at the transmitter or the receiver side.

In Chapter 5, the proposed misalignment concept is presented and its performance is verified through simulations.

Finally, the conclusion and summary of this Thesis are given in Chapter 6.

Chapter 2

Wireless Power Transfer Technique

The WPT technique, based on the transfer distance, can be classified into three categories: near, mid, and far wireless power transfer. In this chapter, these categories will be reviewed. In addition, the theory behind wireless power transfer is presented in this chapter. Besides these, different resonance-based wireless power transfer structures are analyzed in detail.

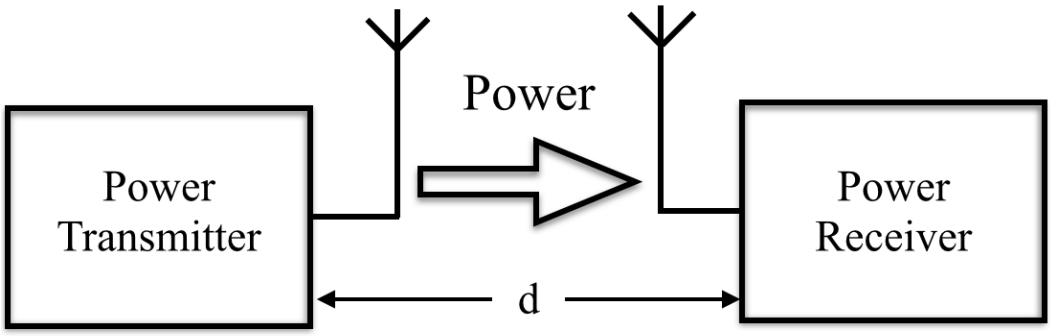

Figure 2.1 The block diagram of wireless power transfer system.

2.1 The Categories of Wireless Power Transfer

The categories are classified based on the working distance, d, between the transmitter and receiver, in the wireless power transfer system in Fig. 2.1. The illustration of these categories is shown in Fig. 2.2. Suppose the wavelength of power transfer is λ, and the transmission distance d is less than $\lambda/2\pi$, $d < \lambda/2\pi$, then the system is classified as

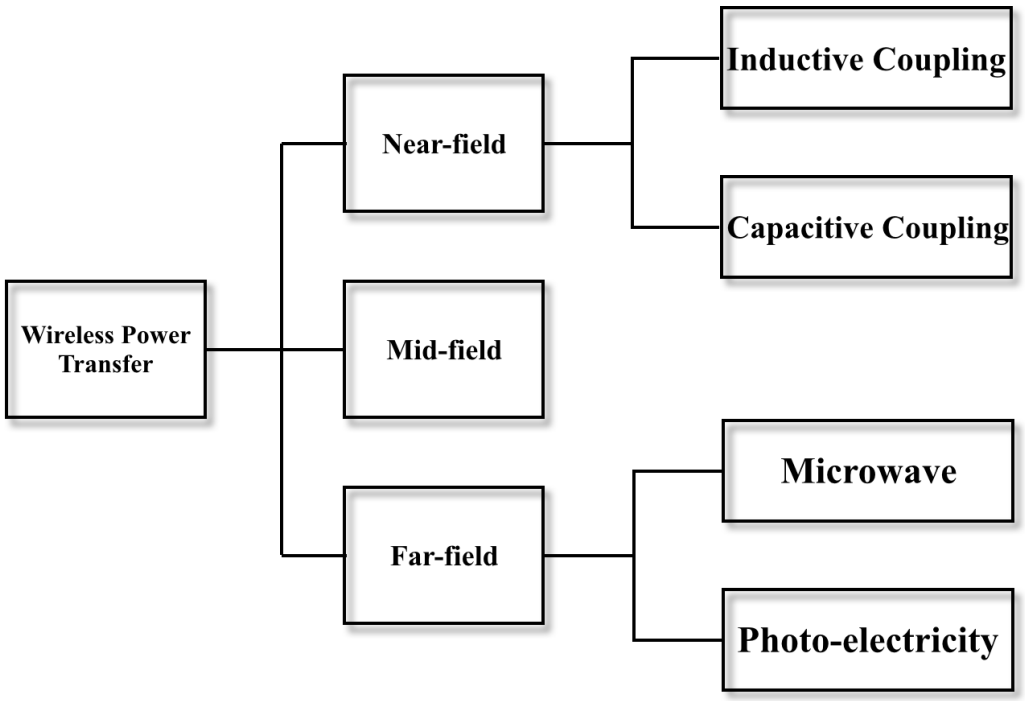

Figure 2.2 The categories of wireless power transfer techniques.

near field. If d is more than λ/π, $d > \lambda/\pi$, it is named as far field. The mid field is classified as d is between $\lambda/2\pi$ and $d > \lambda/\pi$, which is $\lambda/2\pi < d < \lambda/\pi$. The near field WPT system is described first.

2.1.1 Near field wireless power transmission

In near field WPT, the basic power transmission approaches are magnetic induction and electric induction. The next paragraphs will describe them separately.

Wireless power transfer through **electric induction** uses capacitive power transfer (CPT) technique. Due to its small system volume and profile [14], CPT is used in small sized applications such as biomedical applications [15] [16], robots and mobile devices

[17], [18]. In addition, the merits of a cheap and flexible design make the capacitive power transfer to be an appropriate method in moving systems, such as robot arms [19]. Even though the magnetic induction has the advantage of high power transfer efficiency than capacitive power transfer, CPT is the better choice than the magnetic induction under the high operational frequency scenarios [15]. The basic topology of CPT system is shown in Fig. 2.3. The power amplifier is usually adopted as an

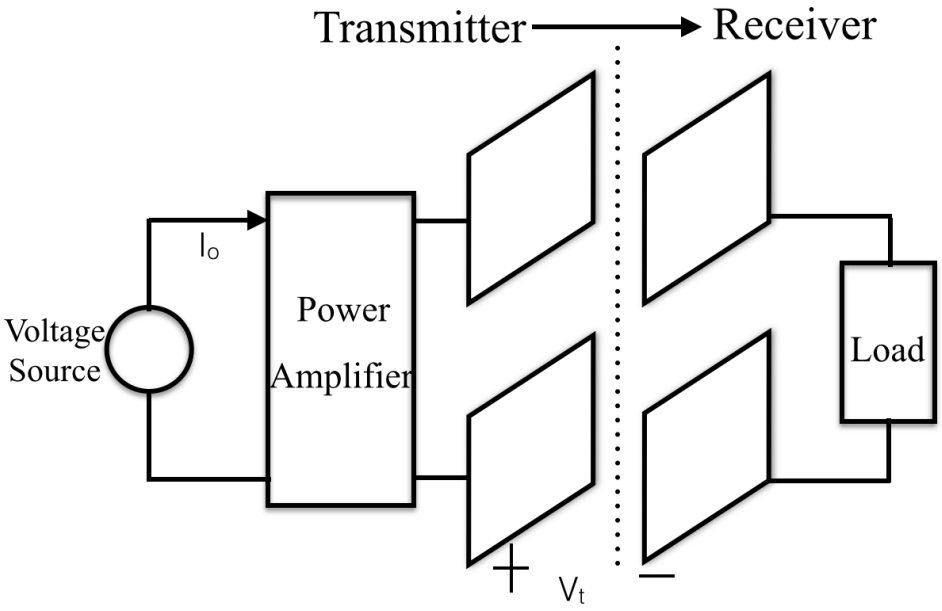

Figure 2.3 The topology of capacitive wireless power transfer system.

inverter. This inverter is utilized to generate AC signal and feeds the signal through a capacitive interface. The power can then be transferred via the system to the load. The capacitance is typically few hundreds picofarads in value [20]. To feed enough current to the interface, in certain systems, inductors are placed before the capacitors [21]. The existing capacitive power transfer systems use large capacitors [17]. The operation theory of capacitive power transfer technique is described as follow.

The alternating voltage signal, which is generated from the power supply and the power

amplifier, is applied to the capacitor. It produces an electric field which can be modeled as:

$$E = \frac{V}{l}. \tag{2.1}$$

Here, V is the voltage applied on the two plates of the capacitor and l is the distance between the two plates. The alternating voltage will induce an oscillating electric field in the capacitor. Due to the electrostatic induction, the alternating electric field can generate a variable potential on the receiver plate. Thus, an alternating current is also generated to feed the load. The transmitted power depends on the frequency and capacitance. In Fig. 2.3, the power which is going to be transferred to the load is expressed as [14]:

$$P = V_t I_o cos(\beta). \tag{2.2}$$

In 2.2 V_t is the voltage across the two plates of transmitter capacitor and β is the phase difference between the voltage V_t and the transmitter current I_o. β and I_o can be derived as [14]:

$$\beta = tan^{-1}(-\frac{1}{\omega C R_{re}}), \tag{2.3}$$

$$I_o = \frac{V_t}{\sqrt{(1/\omega^2 C^2) + R_{re}^2}}, \tag{2.4}$$

where C is the capacitance, ω is the working frequency and the R_{re} is the reflected impedance in the transmitter which is from the receiver. Then the voltage across each capacitor then is found as:

$$V_C = \frac{I_o}{\omega C}. \tag{2.5}$$

Equations (2.2)-(2.5) present the important design parameters. These design factors can be optimized to achieve the best working condition of CPT system.

Currently, CPT is applied in some low power applications. For applications involving high power transfer, the magnetic induction will be used. Additionally, electric fields can interact strongly with some materials, such as human muscle [22]. Therefore, for

powering biomedical implants, the magnetic induction is more widely used instead of electric induction.

Magnetic induction power transfer (MIWPT) is used to transfer power via magnetic field. The magnetic coupling can be defined as two groups, inductive wireless power transfer (IWPT) and resonant wireless power transfer (RWPT) [23]. The inductive wireless power transfer is realized by utilizing non-resonant coupled inductors, such as a conventional transformer. It works on the principle of a primary coil generating a magnetic field due to an AC current and inducing an alternating voltage in the receiver coil. This technique requires that the magnetic field is covered by the receiver coil in short distance and the presence of a magnetic core is necessary. The coupling between the two coils is determined by the distance between the inductors, the shape and the placement angle of the coils. The working theory of this technique is shown in Fig. 2.4. Here, L_1 represents the transmitter coil which is typically to be made as large as possible for transmitting more power. L_2 is the receiver coil to receive the energy. B indicates the magnetic field coupled by the two coils and Z is the distance to transfer the power.

The resonant coupling method is considered to be the most efficient way in wireless power transfer applications [15]. This method requires a resonant transformer. As for the basic two resonator system, it has two high quality factor Q coils connected with capacitors to form two coupled LC circuits. This structure is shown in Fig. 2.5. The resistors R_s and R_c are used to model the parasitic resistors associated with the coils L_s and L_c, respectively.

If these two resonators are placed in proximity to one another such that there is magnetic coupling between them, it becomes possible that the resonators can exchange the energy in high efficiency. When the two resonators work at the same resonant frequency, the

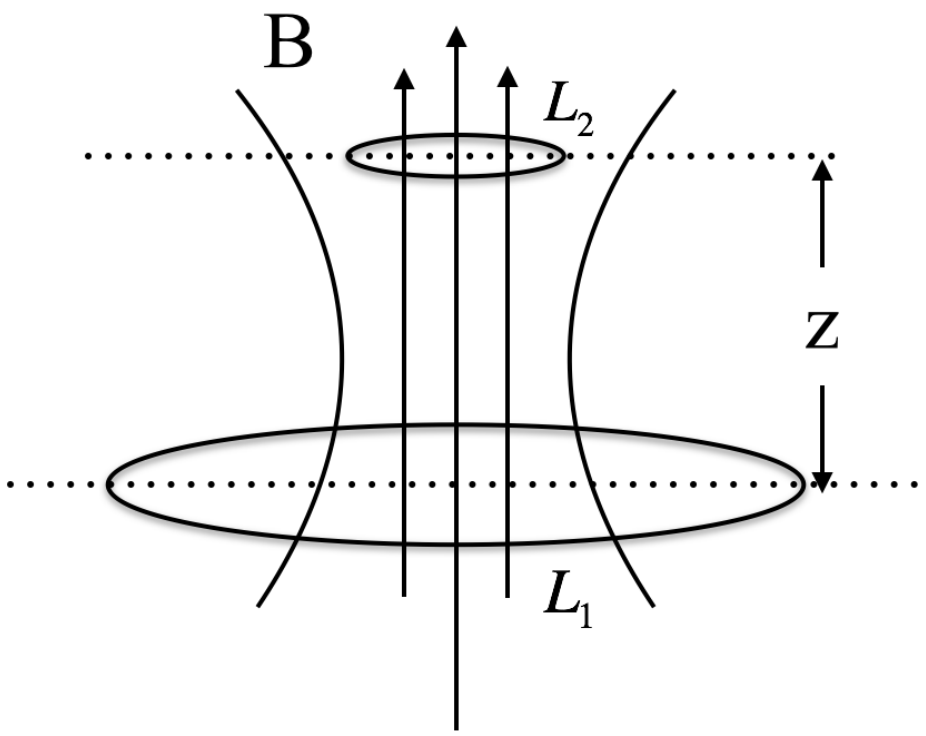

Figure 2.4 Conceptual illustration of the inductive coupling wireless power transfer technique.

energy transfer efficiency can be maximized [15]. In resonant wireless power transfer, an oscillating current is passed through the coils. This current will induce an oscillating magnetic field too. Under the highly resonant situation, the energy is stored in the coils. The biggest disadvantage of non-resonant coupled inductors is the power decaying more server than resonant coupled coils. By using the inductive coupling wireless power transfer, the distance between the two coupled coils needs to be as close as possible. While, using the resonance, this disadvantage can be eliminated, resulting in the improvement of power transfer efficiency.

The power transfer efficiency is highly depended on the coupling factor between the two coils. The system can be mainly classified as four categories based on the coupling coefficient [15]. First is the tight coupling, meaning that the coupling factor is around 1.

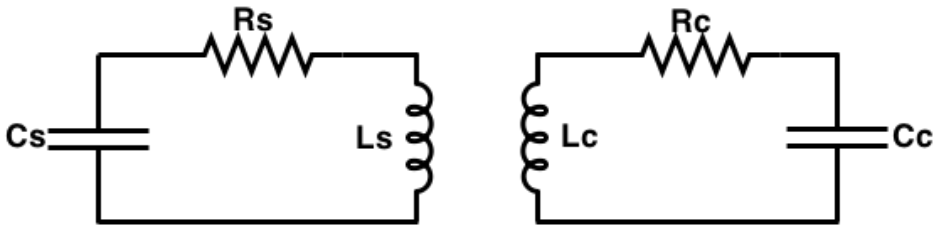

Figure 2.5 Resonance based wireless power transfer structure.

Second is the overcoupling, it happens when the secondary coil is placed so close to the primary coil. The third category is defined as critical coupling. It happens when the power transfer is in its optimum passband. The last category is the loose coupling. It can be seen from its name that in this situation, the coils are far away from each other and the coupling coefficient is much less than the tight coupling. There are different structures to build the resonant wireless power transfer. The detailed information which includes the analysis will be discussed in section 2.2.

2.1.2 Far field wireless power transmission

For achieving power transmission over large distances, the far field wireless power transfer technique is used. It is briefly introduced in this section . Two methods are usually adopted in far field transmission which are microwave and optical electricity.

Microwave transmission uses microwave to transmit power over a long distance. This technique should thank to Nikola Tesla who contributed to the design of modern electricity supply system and demonstrated 'the power transmission without wires' [24]. Basically, this power transmission technique can be divided into three blocks as shown in Fig. 2.6 [25]. First block is to convert DC power to microwave power for making it to be ready transferred. The second block is the link which is used to transfer the

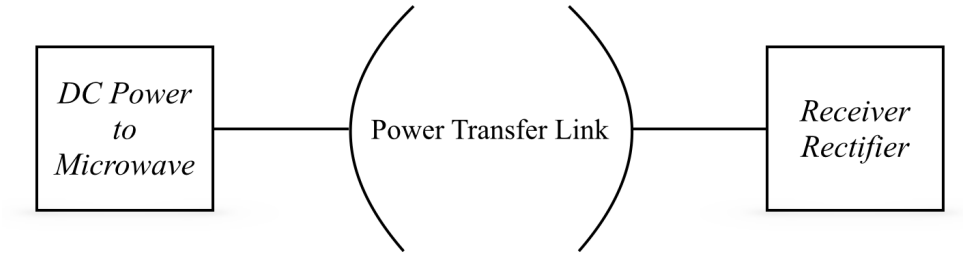

Figure 2.6 Structure of microwave wireless power transmission system.

power. The last one is the receiver block to receive and rectify the power.

These blocks with their interaction determine the power transfer efficiency of the system. For example, if the power transfer efficiency of each block in Fig 2.6 is represented by η_1, η_2 and η_3, the overall power transfer efficiency can be found as:

$$\eta = \eta_1 \eta_2 \eta_3. \tag{2.6}$$

For realizing the power transfer links required in this method, several techniques have been adopted. One of them uses an active phased array [25]. This technique is applied in very large arrays ,such as in space, for maximizing the power transfer efficiency. Another technique, best suited for smaller system, is to combine an ellipsoidal reflector and dual-mode horn. [25].

Optical electricity which uses laser beam, is considered to be another promising approach for realizing the far field wireless power transfer. Even though the power is transmitted using laser, in the receiver side the power still needs to be converted to the electrical energy. There are several advantages for utilizing laser for power transmission [26]:

1 The laser beam can be made as small as possible for small products application.

2 There is no radio frequency interfacing with other communication products such

as phone and wifi by using laser beam.

3 Using laster beam, the amount of transfer power can be controlled .

Even though there are many advantages, the drawbacks of this technique cannot be ignored, which are listed as below:

1 The laser is dangerous even in low power level, it can cause blindness in people and animals.

2 The efficiency for converting the power from light to electricity is low, resulting much power wasted [26].

3 Optical wireless power transfer technique requires a direct line from the transmitter to the target. It is not applicable in certain scenarios.

The far field power transfer technique is a promising way to transmit power wirelessly over a large distance. However, in this thesis, the main discussion is the wireless power transfer for biomedical application which is included in the near field transmission. Therefore, the far field transmission was introduced briefly here. The next section is going to discuss the mid field wireless power transfer.

2.1.3 Mid field wireless power transmission

Mid field power transfer is reported in a recent publication [27]. The power transfer distance of mid field is between near field and far field. It has been approved that it will generate high power transfer efficiency in mid field comparing to near field when the receiver dimension is less than the transmitter [27]. Conventionally, most of the research in near field wireless power transfer using magnetic field are based on applications that use a frequency less than 10 MHz. However, when the receiver size is much smaller than the transmitter, it results in a weak coupling and hence the inductively coupled coils

are inefficient at the lower frequency. Therefore, in [28], it was shown that by utilizing a combination of inductive and radiative modes, higher power transfer efficiency can be achieved in mid field. Also, higher efficiency is achieved by utilizing in low-giga hertz range. However, in mid field wireless power transfer technique, one of the design difficulties is the voltage source for achieving optimum power transfer efficiency.

This section mainly discussed the three categories of wireless power transfer system based on the distance of the power transfer. In each category, the methods for realization are also analyzed in detail. For biomedical implants, the near field is widely used. The resonant power transfer is a preferred approach in biomedical applications. Therefore, in the next section, the structures of resonant power transfer are well analyzed.

2.2 Resonant coupling wireless power transfer structures

In resonance coupling, there are mainly 3 structures: two-coil links, three coil links and four coil links based on the number of coils used. These three structures are widely used in today's near field wireless power applications.

2.2.1 2-Coil based wireless power transfer structure

The two-coil based resonance coupling structure is shown in Fig. 2.7 [1]. A voltage source is added at the transmitter with a source resistor R_s. On the transmitter side, the resonator is formed by a capacitor C_1 and the primary coil L_1. There is also a parasitic resistor R_1, the primary coil at the transmitter side. The receiver resonator is also formed by a capacitor C_p and the inductor L_2. R_2 is the parasitic resistor of L_2. The load is modeled by a resistor R_L.

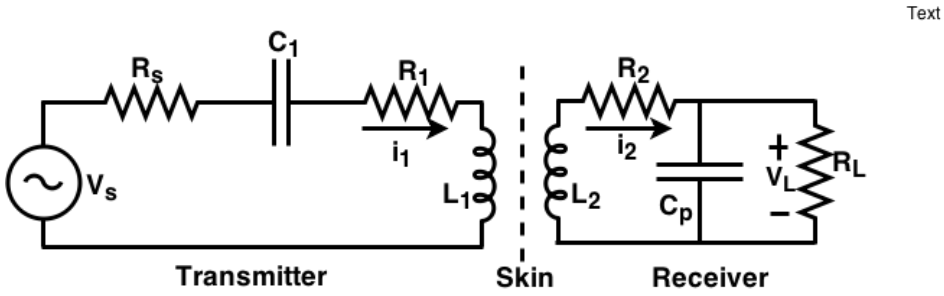

Figure 2.7 Circuit diagram of 2 coil wireless power transfer structure.

The current i_1 which goes through the transmitter coil is a time variant current. It generates a magnetic field. Through the mutual inductance M_{12} between the primary and secondary coil, the magnetic field goes into L_2 and generates the receiver current i_2. The power is transferred by this mechanism. To maximize the transferred power, the working frequency of the transceiver LC resonators needs to be tuned to match each other. The frequency f_o is the resonance frequency of these two resonators:

$$f_o = \frac{1}{2\pi\sqrt{L_1 C_1}} = \frac{1}{2\pi\sqrt{L_2 C_p}}. \tag{2.7}$$

In Fig. 2.7, the voltage across the load V_L can be expressed as [1] :

$$V_L = \frac{j\omega M_{12} i_1}{1 + (j\omega L_2 + R_2)(\frac{1}{R_L} + j\omega C_p)}. \tag{2.8}$$

The authors of [1] compared the load voltage between the structure with resonator and without resonator which indicates that C_1 and C_p are removed in Fig. 2.7. Under the no resonators situations, the voltage across the load $V_L^{'}$ is modeled as [1]:

$$V_L^{'} = \frac{j\omega M_{12} i_1}{1 + \frac{j\omega L_2 + R_2}{R_L}}. \tag{2.9}$$

From the result, it shows that in low frequency range, the voltages in both situations are relatively the same. However, when the frequency goes up to get close to the

resonant frequency, the voltage of resonance coupling becomes higher than the inductive coupling. Then as the frequency goes up, the voltage of inductive coupling is higher than the resonance coupling which is shown in Fig. 2.8.

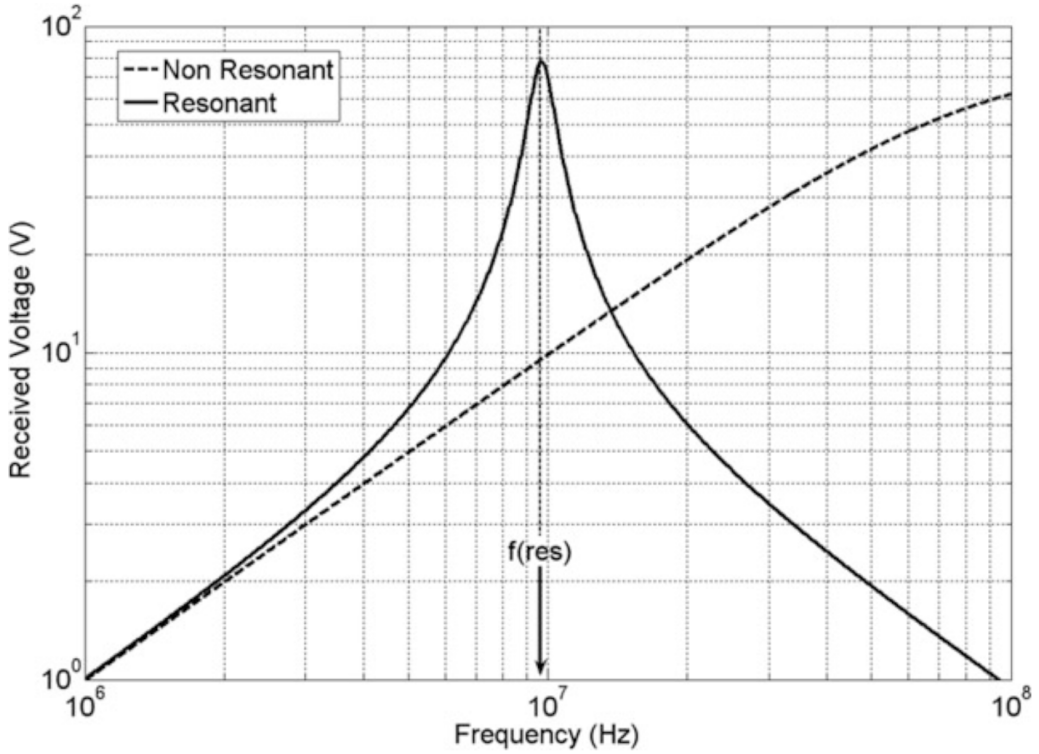

Figure 2.8 The comparison of received voltage across the load between resonant structure and non-resonant structure [1].

By including the quality factor, the power transfer efficiency of the resonant links is [1]

$$\eta = \frac{k_{12}Q_1Q_{2L}}{1+k_{12}^2Q_1Q_{2L}}\frac{Q_{2L}}{Q_L}. \tag{2.10}$$

Here, $Q_1 = \frac{\omega L_1}{R_1}$ is the quality factor of the transmitter. ω is the operational angular frequency of this system. The receiver quality factor is $Q_2 = \frac{\omega L_2}{R_2}$. The load quality factor is expressed : $Q_L = \frac{R_L}{\omega L_2}$. $Q_{2L} = \frac{Q_2 Q_L}{Q_2+Q_L}$ is the combination of Q_2 and Q_L.

The detailed steps for generating the power transfer efficiency can be found in [1]. Even

though the two-coil based structure is widely used by the designers, the power transfer efficiency is low. Therefore, 3-coil and 4-coil structures have been proposed to get more power transfer efficiency. In the next section, the 3-coil structure will be briefly discussed.

2.2.2 3-Coil based wireless power transfer structure

In [29], the three-coil based resonance wireless power transfer structure was successfully implanted. The motivation of designing the three-coil structure is to achieve a high power delivered to the load without hurting the power transfer efficiency because as it will be seen, the four-coil based structure can reach a high power transfer efficiency, but resulting in a low power received by the load.

Comparing with the two-coil structure, an additional resonator is added between the transmitter and receiver to form three-coil power transfer structure. The circuit diagram of three-coil structure is shown in Fig. 2.9. In this structure, the power transfer efficiency η_{3coil} can be expressed as [29]:

$$\eta_{3coil} = \frac{(k_{23}^2 Q_2 Q_3)(k_{34}^2 Q_3 Q_{4L}) + k_{24}^2 Q_2 Q_{2L}}{cos(\theta)(1 + k_{34}^2 Q_3 Q_{4L})\sqrt{A^2 + B^2}} . \frac{Q_{4L}}{Q_L}, \tag{2.11}$$

where, A, B and θ are:

$$A = 1 + k_{23}^2 Q_2 Q_3 + k_{34}^2 Q_3 Q_{4L} + k_{24}^2 Q_2 Q_{2L}, \tag{2.12}$$

$$B = 2 Q_2 Q_3 Q_{4L} k_{23} k_{24} k_{34}, \tag{2.13}$$

$$\theta = tan^{-1}(B/A). \tag{2.14}$$

k is the coupling factor between the inductive coils. k_{23}, k_{34} and k_{24} represent the coupling factor of L_2 and L_3, L_3 and L_4, and L_2 and L_4 respectively. Q_2, Q_3, Q_4 and Q_L represent the quality factor of L_2, L_3, L_4 and the load respectively.

$$Q_2 = \omega L_2 / R_2. \tag{2.15}$$

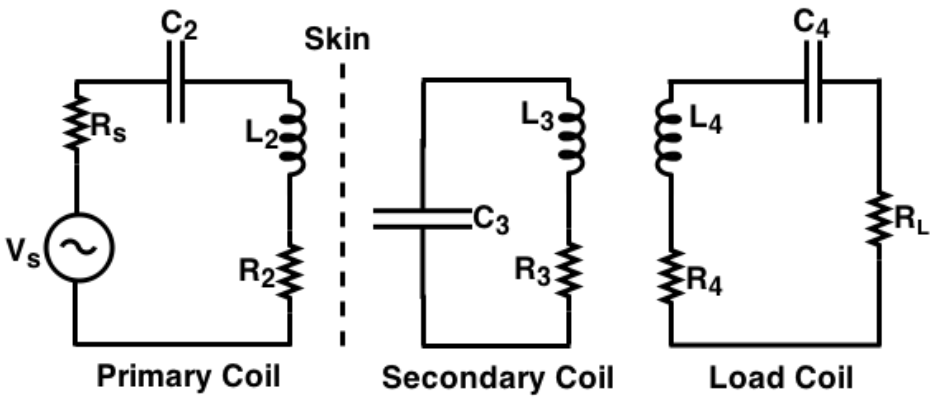

Figure 2.9 Circuit diagram of 3 coil wireless power transfer structure.

$$Q_3 = \omega L_3 / R_3. \tag{2.16}$$

$$Q_L = R_L / \omega L_3. \tag{2.17}$$

$$Q_4 = \omega L_4 / R_4. \tag{2.18}$$

Q_{4L} is the combination of Q_4 and Q_L, as:

$$Q_{4L} = Q_4 Q_L / (Q_4 Q_L). \tag{2.19}$$

Here ω represents the working frequency of these coils. The power delivered to the load, P_L, can be computed as:

$$P_L = \frac{V_s^2}{2R_2} \frac{(k_{23}^2 Q_2 Q_3)(k_{34}^2 Q_3 Q_{4L}) + k_{24}^2 Q_2 Q_{2L}}{A^2 + B^2} . \frac{Q_{4L}}{Q_L}. \tag{2.20}$$

where V_s is the power source which comes from power supply and R_2 is the parasitic resistance of L_2. Due to the large distance between L_2 and L_4, the coupling factor k_{24} can be ignored, therefore the equations of power transfer efficiency η'_{3coil} and power

delivered to the load $P_L^{'}$ can be simplified as below:

$$\eta_{3coil}^{'} = \frac{(k_{23}^2 Q_2 Q_3)(k_{34}^2 Q_3 Q_{4L})}{(1 + k_{34}^2 Q_3 Q_{4L} + k_{23}^2 Q_2 Q_3)(1 + k_{23}^2 Q_2 Q_3)} . \frac{Q_{4L}}{Q_L}, \tag{2.21}$$

$$P_L^{'} = \frac{V_s^2}{2R_2} \frac{(k_{23}^2 Q_2 Q_3)(k_{34}^2 Q_3 Q_{4L})}{(1 + k_{34}^2 Q_3 Q_{4L} + k_{23}^2 Q_2 Q_3)^2} . \frac{Q_{4L}}{Q_L}. \tag{2.22}$$

The merits of this structure comparing with the 2-coil system are by adding additional resonator between the primary and secondary coil, it provides another design freedom to be adjusted to reach the optimum performance. Also, the parameters L_3, L_4 and the coupling factor k_{34} can be utilized to form an impedance matching circuit. The high power transfer efficiency can be achieved under any load R_L. In addition, by optimizing k_{23} and k_{34}, the optimum power delivered to the load can be computed based on (2.21).

2.2.3 4-coil based wireless power transfer structure

The four-coil structure in Fig. 2.10 has been widely used recently [29]. Comparing with the 3-coil structure, four-coil links is achieved by adding another additional resonator between the transmitter coil and receiver coil. It can mitigate the adversely affect of the small coupling factors between the transceiver [29]. The basic four-coil structure is shown in Fig. 2.10. Here the transmitter coil is modeled as L_1 and the remain

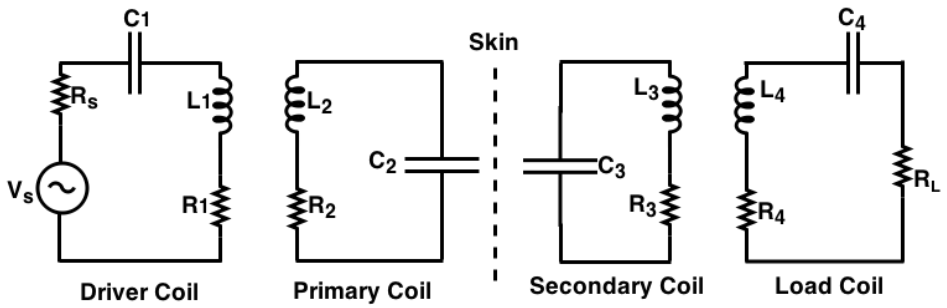

Figure 2.10 Circuit diagram of 4 coil wireless power transfer structure.

components are similar to the ones in Fig. 2.9. The main goal of this structure is to maximize the power transfer efficiency η_{4coil} [13]. It can be expressed as:

$$\eta_{4coil} = \frac{(k_{12}^2 Q_1 Q_2)(k_{23}^2 Q_2 Q_3)(k_{34}^2 Q_3 Q_4)}{[(1+k_{12}^2 Q_1 Q_2)(1+k_{34}^2 Q_3 Q_4)+k_{23}^2 Q_2 Q_3][1+k_{23}^2 Q_2 Q_3+k_{34}^2 Q_3 Q_4]}. \quad (2.23)$$

The symbols Q_1, Q_2, Q_3, Q_4, k_{12}, k_{23} and k_{34} in (2.22) have the similar expressions as in (2.15). To achieve the goal of optimizing the power transfer efficiency, the quality factors of this structure are needed to be designed as high as possible [13]. Also the power transfer efficiency can be simplified as:

$$\eta_{4coil}^{'} = \frac{k_{23}^2 Q_2 Q_3}{1+k_{23}^2 Q_2 Q_3}. \quad (2.24)$$

Based on (2.23), the quality factors of the transmitter coil and receiver coil do not have a big impact on the power transfer efficiency. Therefore, by carefully designing the primary and secondary coils, the maximize power transfer efficiency can be obtained.

2.3 Conclusion

In this chapter, modern technique for wireless transferring power were reviewed. Based on the power transfer distance, three categories of wireless power transmission are defined. For the biomedical application, the near filed wireless power transmission is widely used. The newly introducer mid field wireless power transfer technique was also described in this chapter. Due to the advantages which introduced in this chapter, the resonance structure has been adopted to be used for wireless power transfer in biomedical implants. Different types of resonance coupling structures are introduced, which are 2-coil, 3-coil and 4-coil resonance based wireless power transfer structures.

Chapter 3

Coupled Coil Misalignment Analysis

For biomedical applications, the inductively coupled coils in wireless power transfer are designed to maximize the power transfer efficiency. Most of the studies work on the ideal case that the inductive coils are perfectly aligned with each other. However, when the receiver coils are implanted in the human body, the position of receiver coils can be easily changed due to the movement of human body. This results in the misalignment between transmitter coil and receiver coil. Coil misalignment changes the mutual inductance of the coupled coils and effectively degrades the performance of the wireless power transfer system, such as reducing the delivered power and the power transfer efficiency. Therefore, the effect of the coils misalignment is important and needs to be investigated.

In this chapter, we present the analysis of coils misalignment. Different misalignment situations are discussed and the mutual inductance between the coupled coils under misalignment is analyzed.

3.1 Mathematical Model of Coils Misalignment

3.1.1 Misalignment analysis review

In the inductive links, the primary coil generates magnetic field and the receiver coil picks up a part of the magnetic field for power transfer. The system needs to be robust

enough for immunizing the misalignment. To obtain the optimum performance, the coupled coils in the system has been carefully designed. For example, the design in [30] focused on steady-state circuits analysis and the results were validated by experiment.

Some work presented the analysis of the mutual inductance under misalignment. In [31], [32], the detailed analysis of the mutual inductance of coupled coils were presented and using the functions in [31], [32] the mutual inductance value was numerically obtained. [33] and [34] investigated the situations of coupled coils misalignment by computing the mutual inductance. [34] got the results by renewing the conventional numerical equations and [33] generated the results by conducting experiments.

Recently, there are few publications which presented the misalignment effect in mutual inductance of the coupled coils. In this research work, we adopted the approaches in [30] and [35] to analyze the misalignment and the mutual inductance in detail.

3.1.2 Mutual inductance analysis under misalignment

In the ideal case, the positions of coupled coils are aligned with each other. This situation is shown in Fig. 3.1, which shows the cross view of the coils. In the perfect alignment scenario, the coils are positioned in parallel to each other with their center points aligned. The radius of the primary and secondary coils are presented with R_p and R_s, respectively. c denotes the vertical distance between the primary and secondary coil. In practice, the coils cannot typically stay steady in this ideal situation.The positions of the coils may be altered because of the change in the environment, resulting in the misalignment. The misalignment can be mainly categorized into two scenarios which are going to be discussed below.

One of the most common cases is the angular misalignment. This situation is illustrated

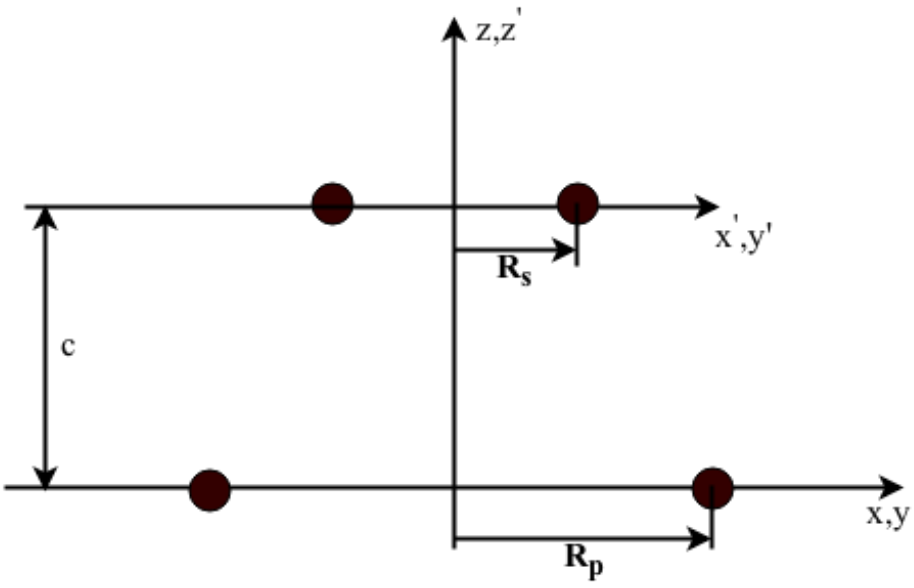

Figure 3.1 Conceptual illustration for coils with no misalignment.

in Fig. 3.2.In this scenario, the center point of the two coils remain aligned, however, the secondary coil has been rotated by an angle θ from its ideal position. In this case, the mutual inductance can be computed as [35]:

$$M = \frac{\mu_o}{\pi}\sqrt{R_s R_p}\int_0^{\pi}\frac{\psi(k)}{\sqrt{V^3}}d\phi. \tag{3.1}$$

where

$$V{=}\sqrt{1-cos^2(\phi)sin^2(\theta)},$$
$$k^2{=}\frac{4\alpha V}{1+\alpha^2+\beta^2+2\alpha\beta cos(\phi)sin(\theta)+2\alpha V},$$
$$\alpha{=}\frac{R_s}{R_p},\ \beta{=}\frac{c}{R_p},$$
$$\Psi(k){=}(\frac{2}{k}-k)K(k)-\frac{2}{k}E(k){=}Q_{1/2}(x),\ x{=}\frac{2-k^2}{k^2}.$$

From (3.1), if the angle θ equals to 0, $cos(\theta)$ is 1, which indicates the perfectly aligned scenario.

Another possible scenario for the misalignment is illustrated in Fig 3.3. Here, in addition to rotation there is a shift d in the axial position of the secondary coil. In this situation,

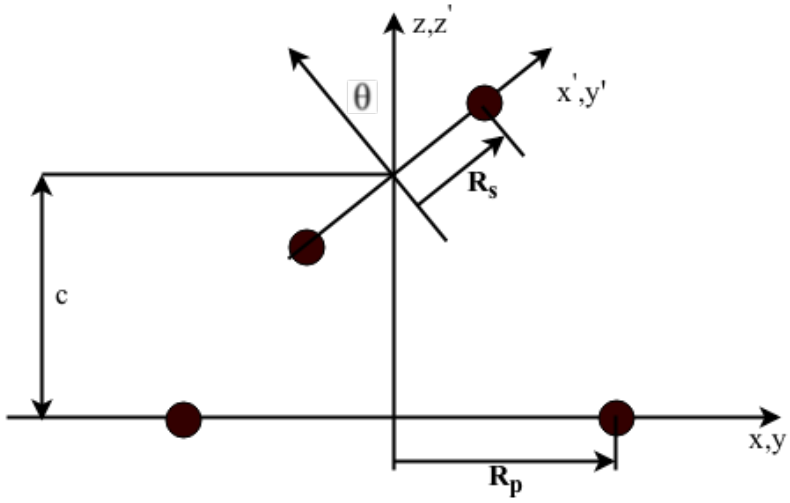

Figure 3.2 Conceptual illustration for coils with angular misalignment.

the mutual inductance in (3.1) needs to be revised accordingly. The new expression for mutual inductance is [35]:

$$M = \frac{\mu_o}{\pi}\sqrt{R_s R_p}\int_0^{\pi} \frac{[cos(\theta) - \frac{d}{R_s}cos(\phi)]\psi(k)}{\sqrt{V^3}}d\phi. \tag{3.2}$$

where

$$V=\sqrt{1 - cos^2(\phi)sin^2(\theta) - 2\frac{d}{R_s}cos(\phi)cos(\theta) + \frac{d^2}{R_s^2}},$$
$$k^2=\frac{4\alpha V}{(1+\alpha V)^2+\xi^2},\ \xi=\beta - \alpha cos(\phi)sin(\theta),$$
$$\alpha=\frac{R_s}{R_p},\ \beta=\frac{c}{R_p},$$
$$\Psi(k)=(\frac{2}{k} - k)K(k) - \frac{2}{k}E(k)=Q_{1/2}(x),\ x=\frac{2-k^2}{k^2}.$$

In the above equations, μ_o is the magnetic permeability of vacuum. Its value is $4\pi\times10^{-7}$ H/m. $K(k)$ and $E(k)$ are the complete elliptic integral of the first kind and second kind [36], [37] respectively. $Q_{1/2}(x)$ is the Legendre function of the second kind and half-integral degree [36].

Basically, in (3.2), the parameter d is incorporated, taking into account that the center of

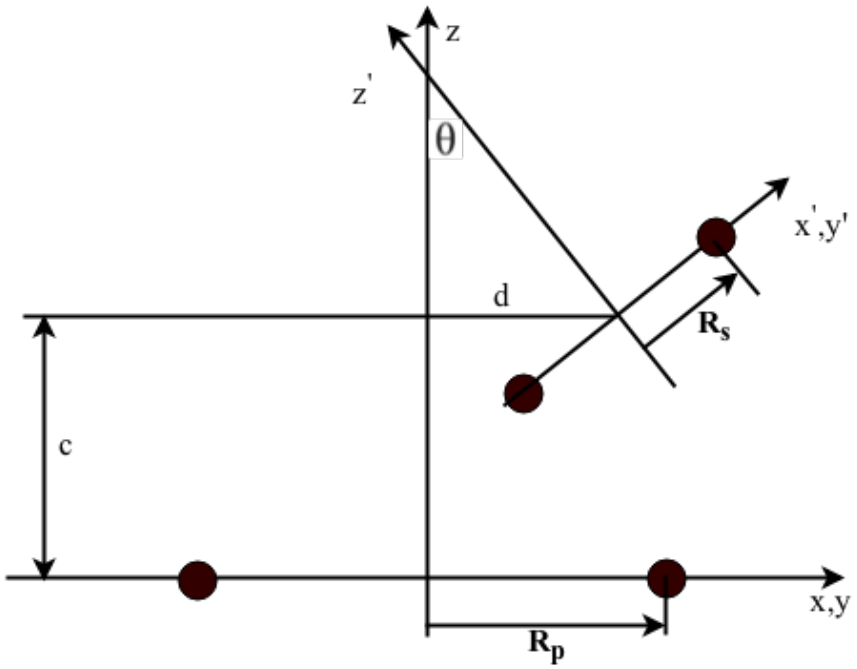

Figure 3.3 Conceptual illustration for coils with angular and axial misalignment.

the coils has deviated from each other. From (3.2), it can be seen that the direct impact of the misalignment is to change the mutual inductance between the two coils.

3.1.3 Calculation of mutual inductance

Several research groups have proposed methods to solve the numerical equations to obtain the mutual inductance values [36], [37]. One of the methods is summarized here.

In this method [2], MATLAB was used to calculate the mutual inductance. The main idea is to divide the total computing program into different blocks which are based on (3.1) and (3.2) [35]. This approach is considered an efficient way to calculate the mutual inductance. This method is summarized in Fig. 3.4.

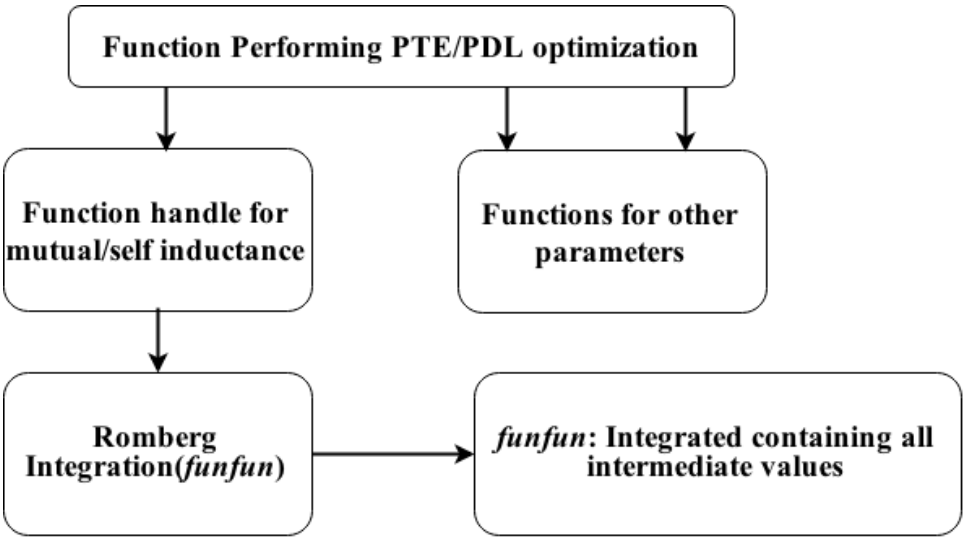

Figure 3.4 The order for functions to perform mutual inductance calculation [2].

A predefined Romberg's Method function is adopted to solve (3.2). Additionally, this method can be used to estimate definite integrals in (3.1), (3.2), which has the integration domain from 0 to π. To obtain the values of mutual inductance, these integrals need to be performed. The variable $funfun$ is used to describe the integrand, which contains variable ϕ and some other intermediate values V, k_2 and $\Psi(k)$. The integration domain is the same as (3.1), (3.2) which is from 0 to π.

3.2 Conclusion

Based on the results which are shown in [35], the mutual inductance can change due to the misalignment in the position of the two coupled coils. In this chapter, we reviewed two common misalignment scenarios. Additionally, to help the coil designer, in the last section, a method for calculating the mutual inductance was also reviewed. Knowing that misalignment is one of the important issue in wireless power transfer system, methods for compensating this effect needs to be developed.

Chapter 4

Misalignment Compensation Work Review

Recently, wireless power transfer technique implemented using inductive links has been widely used in different applications, including radio indentification (RFID) and biomedical implants. The stability of the transferred power is important in these applications, especially in biomedical implants. To make sure the biomedical implant operates properly, the variation in the power supply should be minimized [4]. This consideration increases the difficulty in designing wireless power transfer structures. As discussed in Chapter 3, an factor which can impact the stability of the power transfer is the misalignment in the position of coupled coils. To address the misalignment issues, different compensation methods have been proposed.

This chapter presents a literature review of the technique that have been used to address the misalignment problem. Majority of the approaches try to tune some design parameters of the system to mitigate the negative impact of misalignment. Mostly, the parameters on the transmitter side are tuned because in biomedical implants it is easier to add extra elements on the external side than on the receiver side, considering the space limitation of the implant. Based on the parameters tuned, the compensation approaches can be classified into different categories. These are discussed in next sections.

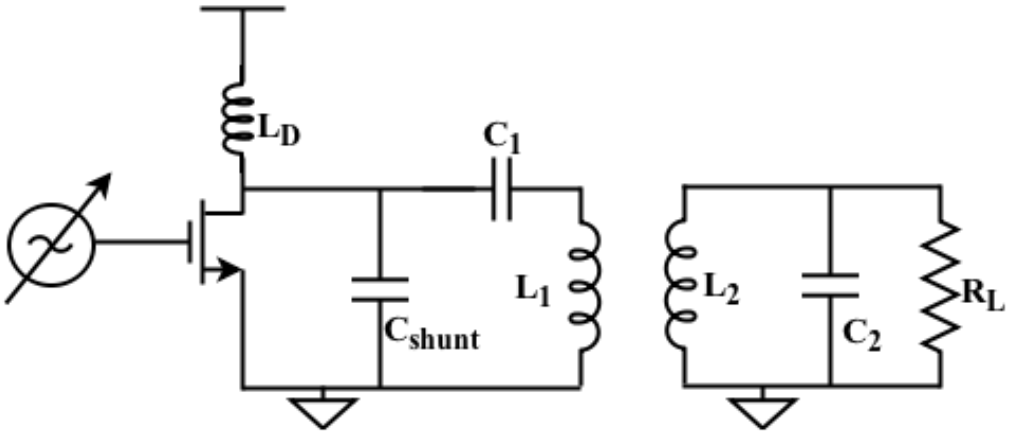

Figure 4.1 Frequency control compensation technique [3].

4.1 Frequency control methods

The misalignment is caused by the displacement or the distance deviation of the coils. One of the possible methods to solve the misalignment issue is the frequency control technique. Fig. 4.1. illustrates the circuit diagram for this method [3]. It includes a class E power amplifier as the driver circuit. The two-coil resonance structure is adopted.

The switching frequency control method has been proposed in [3]. By computing the equations of the structure, the authors proposed that the frequency can be tuned to mitigate the negative effect of misalignment. However, based on the analysis in [3], it is demonstrated by the authors that the drain inductor needs also to be altered to cope with the frequency tuning which is not necessary. Also, the authors only focus on the class E power amplifier without targeting the power delivered to the load.

Another method to change the frequency was implemented in [4]. In this paper, the authors mainly focus on the class E power amplifier analysis. First, the different load versions of class E power amplifier was analyzed. An optimum load structure was

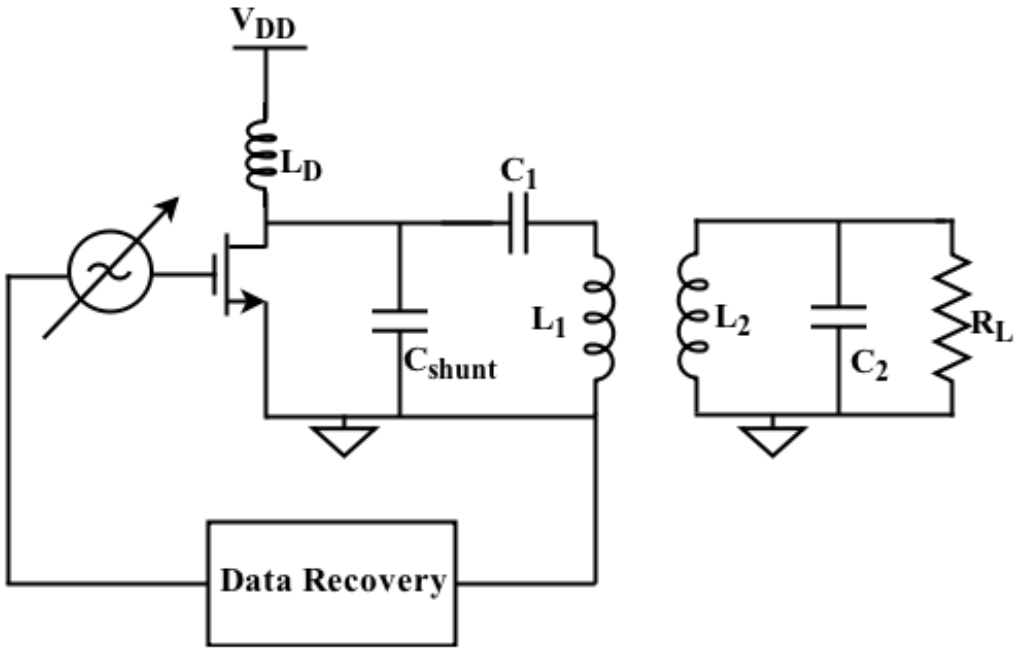

Figure 4.2 Closed loop gate control technique [4].

selected. Then, the authors proposed a method to sense the current change at the transmitter side. A closed loop structure had been implemented as shown in Fig. 4.2. By obtaining transmitter current, the operational frequency of this circuit was adjusted accordingly. Similar to [3], in this paper, the authors did not address the power reduction problem to the load due to misalignment. Besides the frequency, the power supply in the transmitter can also be altered to do the compensation.

4.2 Power supply control methods

Since the power transfer efficiency of coupled coils is related to the working frequency [5], changing the operational frequency of the coils will impact the power transfer efficiency. Therefore, other methods to solve the misalignment problem were proposed. It is proved that changing the power supply at the transmitter side could be a promising way to

compensate the misalignment effect.

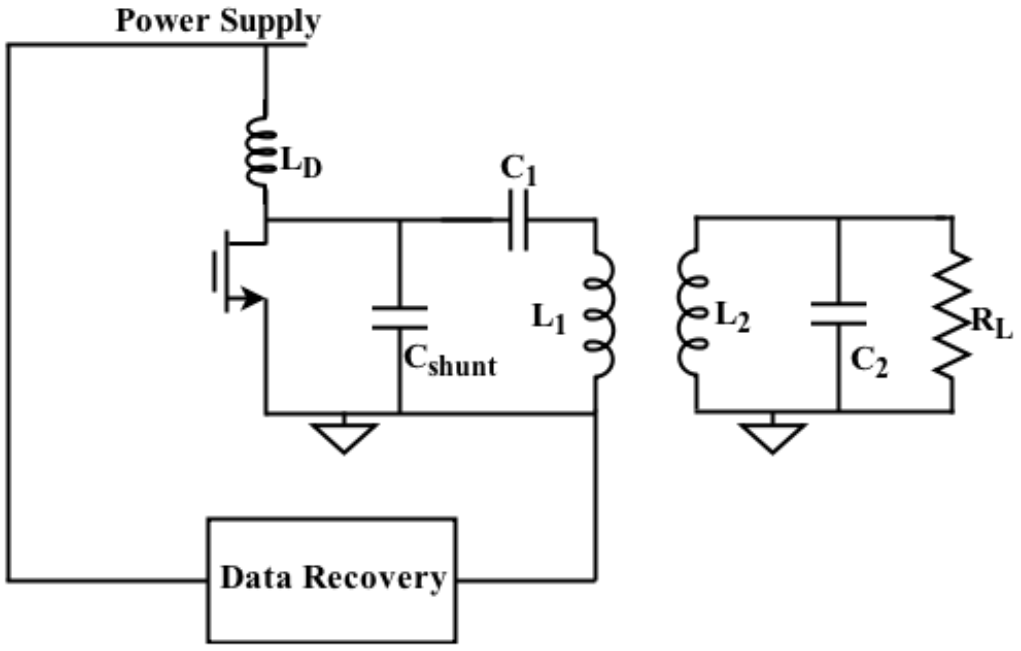

Figure 4.3 Closed loop power control technique [5].

A typical structure in retinal prosthesis was developed in [38] and is shown in Fig. 4.3. It was also designed as a closed loop structure. The two coil resonant structure driven by a class E power amplifier was adopted. A reverse telemetry block was added at the receiver side to send data to the transmitter. By sensing the current at the transmitter side using a current transformer, the variation of the load of the system can be calculated. Additionally, the sensed current is used to set the power supply at the transmitter side. This system was shown to deliver constant power 250 mW to the load by tuning the power supply. In addition, mathematical model of this system was developed to analyze its stability.

In [6], an adaptive wireless power transfer system which for use in biomedical implants was designed to control the power under different situations. A real time signal from

an implant in moving animal was monitored. There is an implanted coil in the animal which is the secondary coil. The animal was placed in a cage and the primary coil is on the cage. The primary and secondary coils are used to transfer power. Due to the movement of the animal, the coupling factor between the coupled coils changes continuously. Therefore, the system needs to immunize the problem of a change of coupling factor. To detect the change in the delivered power, a power sensing block was implemented at the receiver side which is shown in Fig. 4.4. It was achieved by comparing the regulator voltage to a reference voltage. Then the data was transferred to the transmitter side. According to the back telemetry data, the power supply was controlled to deliver a stable power.

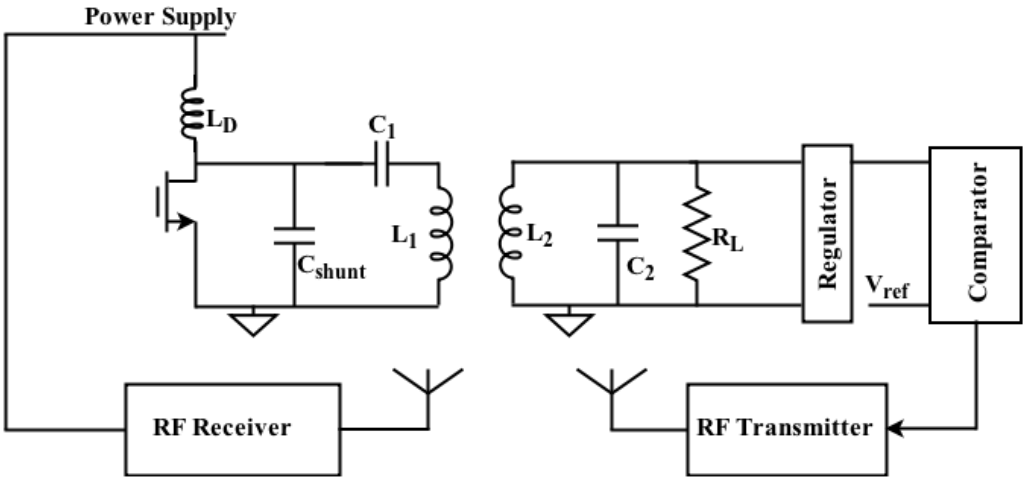

Figure 4.4 Closed loop power control technique implementing by a comparator and RF transceiver [6].

Another design example was also illustrated in [39]. The design uses a closed loop structure which is similar to Fig. 4.4. This structure was implemented by a radio frequency (RF) transceiver on both receiver and transmitter side. The design structure on the receiver side was similar to [6]. It picked up and detected the regulated voltage to generate the information about the change in power. The information data was sent

to the external side via the RF transceiver. Based on the received data, the power supply was changed accordingly. This system generated 10-30.2 dBm power with a high efficiency of around 71.5 %. In the next section, the misalignment issue can also be mitigated by using the off-the-shelf microcontroller.

4.3 Microcontroller control methods

[7] describes to use off-the-shelf components to build wireless power transfer system. It is a closed loop structure for biomedical implants. Several off-the-shelf components were included in this system, such as an RFID Transceiver, a DC-DC converter and a microcontroller. The system which is shown in Fig. 4.5 was operating at 13.65 MHz, generating a stable 11.2 mW output power to the load via a large range. To detect the variation of receiver power, microcontrller (MSP430) was connected to the regulator. It is also used to detect the regulated voltage and control the back telemetry block in the receiver to send the data. The control unit was built to alter the supply voltage of the RFID transceiver (TRF 7960). It was designed by only using off-the-shelf components: microcontroller (MSP 430), digital potentiometer (CAT5113) and DC-DC converter (TPS 61070). Similar to [38], mathematical model of the system was also presented for analyzing the stability. By changing the transfer power range from 0.5 to 2 cm, the off-the-shelf components system can still deliver constant power at 13.65 MHz.

4.4 Conclusion

In this Chapter, different misalignment compensation methods were reviewed in detail.

First, by controlling the gate drive signal of the system, the working frequency and the duty cycle of the control signal can be altered to mitigate the misalignment effect.

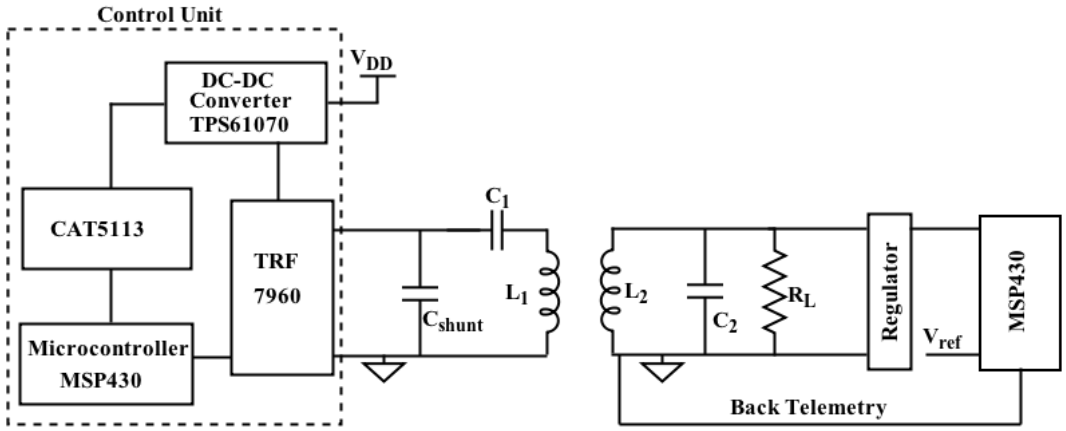

Figure 4.5 Block diagram of microcontroller control technique [7].

Second, the method for altering the supply voltage was proposed. Most of them were implemented by a closed loop structure. It is demonstrated that the closed loop was designed on the transmitter side by adding a current transformer. It is also indicated that adding an RF transceiver on the receiver and transmitter is a way to sense the misalignment. The output data can be transferred via the RF transceiver. Then in the power transmitter side, the power supply is changed according to the data received.

Finally, it takes advantage of off-the-shelf components to build the wireless power transfer system. The misalignment compensation can be achieved by programming these devices. Off-the-shelf microcontroller can also read data and build a back telemetry structure for data transfer. A design example was analyzed to present the performance of off-the-shelf components.

Comparing these proposed methods of compensation, a novel concept for solving the coil misalignment issue is introduced in the next section.

Chapter 5

Proposed Concept for Coils Misalignment Compensation

The misalignment between the primary and secondary coils could naturally occur as a result of body movement or changes in the biological environment. An immediate effect of coil misalignment is the reduction in the power delivered to the load. In this section, we present a design concept that could be implemented on the transmitter side, to mitigate this effect while keeping the driver to work at its optimum operating condition. Specifically, we will demonstrate analytically and through simulations, that tuning the shunt capacitor and the supply voltage at the transmitter side could be a promising approach to compensate the performance degradation induced by coil misalignment in WPT links.

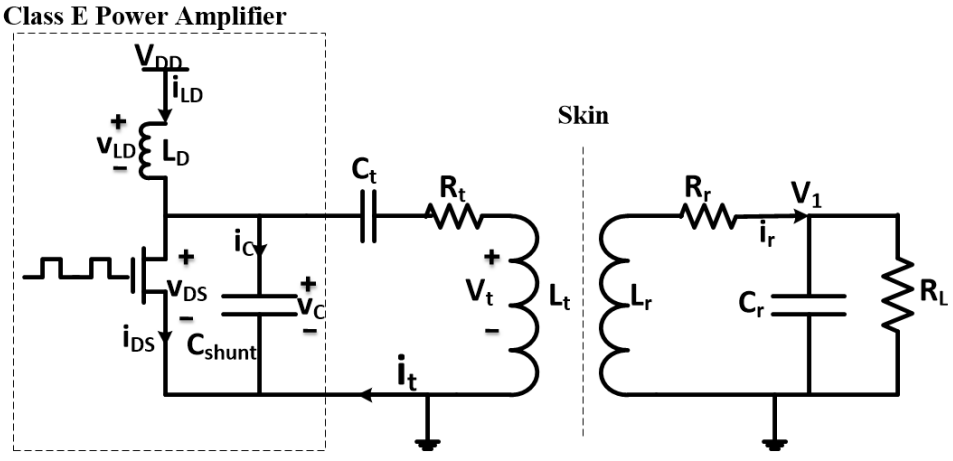

Figure 5.1 Adopted circuit model for wireless power transfer system.

5.1 Circuit Theory Analysis

The circuit of the adopted wireless power system is shown in Fig. 5.1. It is a two-coil based resonance structure. The primary coil L_t and capacitor C_t form the transmitter resonator. R_t is modeled as the parasitic resistance of the primary coil which cannot be ignored [40]. As for the receiver side, the receiver coil is modeled as L_r, receiving the transmitted power. The coil L_r and the capacitor C_r form the resonator in the receiver side. The resistor R_r is used to model the parasitic resistor of L_r. The load resistance is modeled as resistor R_L. In this section, first, the receiver circuit is analyzed. The voltage across the load is computed. Second, the reflected impedance theory is introduced. At last, the working condition of the class E amplifier is discussed to generate the proposed compensation approach.

5.1.1 Receiver circuit

The power transfer is based on the two coupled coils as shown in Fig. 5.2. A time variant current i_t goes through the transmitter coil L_t. This current generates a time variant magnetic field. Part of the magnetic field is picked up by the second coil L_r. Due to the mutual coupling between these two coils, the time variant magnetic field in the receiver coil, L_r, produces an induced voltage. This voltage will be the source at the receiver. The induced voltage is given as:

$$V_{ind}(\omega t) = M_{rt}\frac{di_t(\omega t)}{d\omega t}. \tag{5.1}$$

Here, M_{rt} is the mutual inductance between the transmitter coil L_t and the receiver coil L_r. ω is the operational angular frequency. The M_{rt} can be expressed as:

$$M_{rt} = k\sqrt{L_t L_r}, \tag{5.2}$$

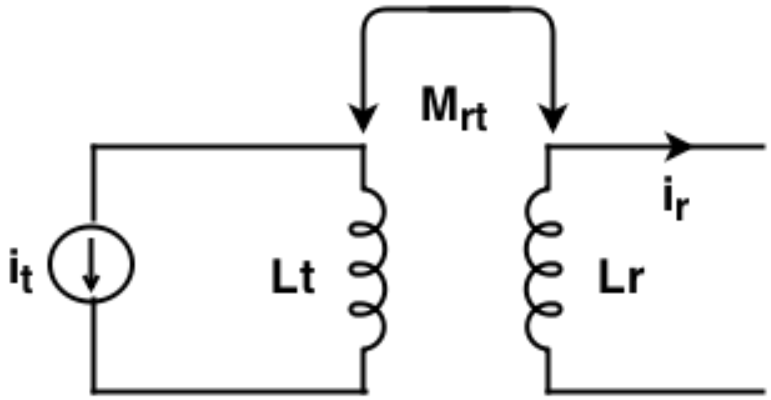

Figure 5.2 Illustration of magnetic coupling working theory.

where k is the coupling factor of the two coils. The induced voltage could be modeled at the receiver side as shown in Fig. 5.3.

At the receiver circuit, the voltage across the load R_L can be computed. The capacitor C_r is paralleled with the load R_L. By using the voltage divider theory, the load voltage can be computed as:

$$V_{load} = V_{ind}\frac{|Z_{load}(\omega)|}{|Z_{total}(\omega)|}, \tag{5.3}$$

where Z_{load} is the total load impedance, Z_{total} is the total impedance of the receiver. They can be computed as:

$$|Z_{load}| = |X_{C_r}//R_L| = \frac{R_L}{\sqrt{1+(\omega R_L C_r)^2}}, \tag{5.4}$$

$$Z_{total} = R_{real} + jX_{ima}. \tag{5.5}$$

R_{real} and X_{ima} are the real and imaginary parts of Z_{toal} respectively. They are expressed as:

$$R_{real} = \frac{R_L}{1+\sqrt{\omega R_L C_r}} + R_r, \tag{5.6}$$

$$X_{ima} = \frac{\omega(L_r - C_r R_L^2)}{1+(\omega R_L C_r)^2}. \tag{5.7}$$

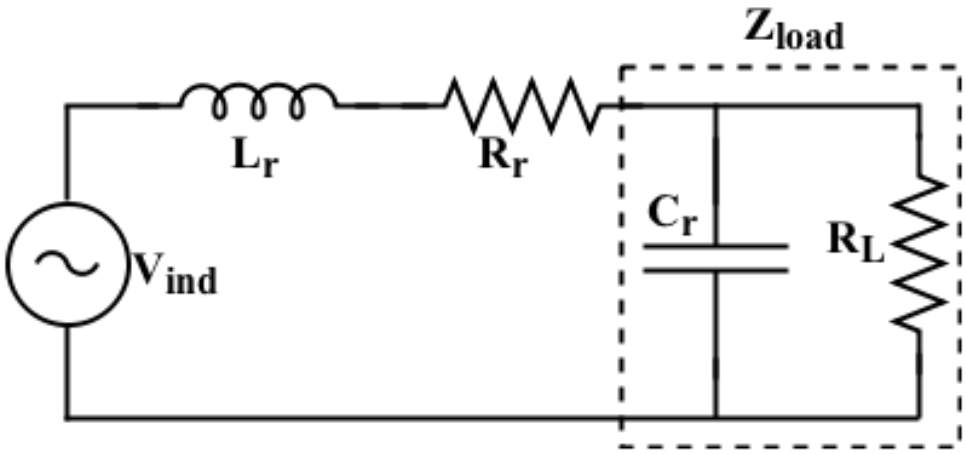

Figure 5.3 The circuit diagram of WPT receiver.

Normally, the current goes into the transmitter is a sine waveform. Therefore, the induced voltage V_{ind} is also a sine waveform. The power P received by the load can be expressed as:

$$P = \frac{V_{load_{peak}}^2}{2R_L}. \tag{5.8}$$

In this case, the load resistance R_L is fixed. The factor to change the received power is the peak voltage of the load $V_{load_{peak}}$. To derive this parameter, the peak value of induced voltage needs to be computed. It is expressed as:

$$V_{ind_{peak}} = M_{rt} I_m = k\sqrt{L_r L_t} I_m, \tag{5.9}$$

where I_m is the value of peak current of the transmitter current i_t. Therefore, the load peak voltage can be derived:

$$V_{load_{peak}} = k\sqrt{L_r L_t} I_m \frac{|Z_{load}(\omega)|}{|Z_{total}(\omega)|}. \tag{5.10}$$

One of the design goals is to ensure that the load receives enough stable power. It means that the peak voltage of the load needs to be stable. From (5.10), it can be seen that the peak voltage of the load is highly related to the coupling factor. Under the

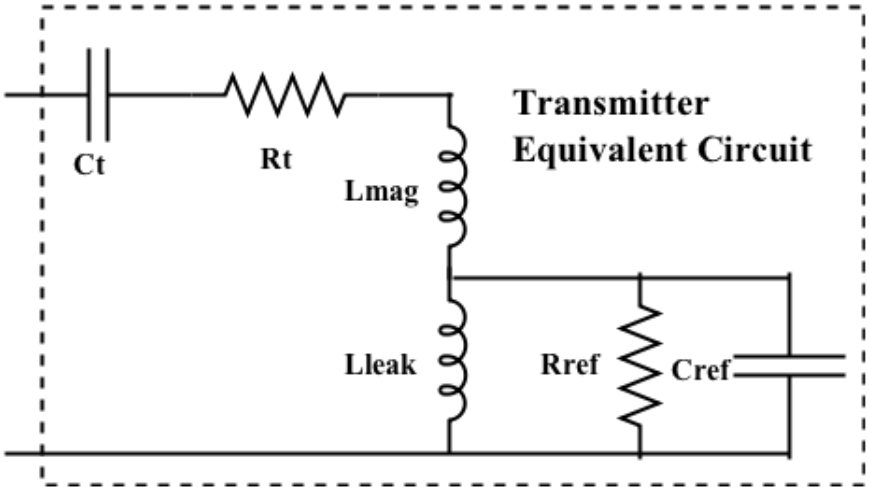

Figure 5.4 Equivalent circuit seen at the transmitter employing reflected impedance theory.

condition of misalignment, the coupling factor is changed resulting in a variable peak voltage of the load which is supposed to be stable in our design.

5.1.2 Reflected impedance theory

Reflected impedance theory is widely used in most wireless power transfer structures. A detailed analysis of this theory was presented in [41]. This theory helps the designer to analyze the wireless power transfer structure easily.

Employing the reflected impedance theory, the equivalent circuit at the transmitter side is shown in Fig. 5.4. The resonant capacitor C_t and the parasitic resistors R_t are kept the same as shown in Fig. 5.4. The transmitter coil is divided into two parts, one is the magnetizing inductor L_{mag} and the other is the leakage inductor L_{leak}. The reflected components are R_{ref} and C_{ref} paralleled with the leakage inductor L_{leak}. To compute the expressions of these reflected components, the receiver circuit also needs to be simplified. The simplified receiver circuit is shown in Fig. 5.5. The parasitic impedance of the receiver coil R_r is converted to an equivalent resistor R_{eq} paralleled

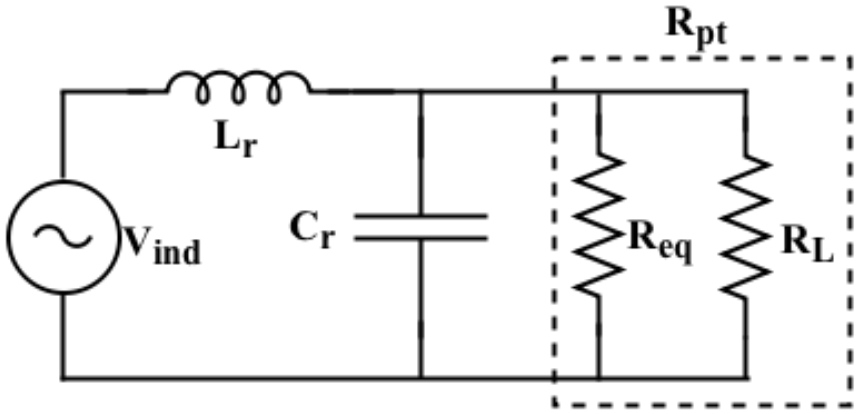

Figure 5.5 The circuit diagram for a simplified receiver in WPT system.

with the load resistor. The equation of R_{eq} is

$$R_{eq} = Q_r^2 R_r. \tag{5.11}$$

Here, Q_r is the quality factor of the receiver coil.

$$Q_r = \frac{\omega L_r}{R_r}. \tag{5.12}$$

R_{pt} as shown in the Fig. 5.5 is the total impedance of the two paralleled resistor R_{eq} and R_L. It equals to $R_{eq}//R_L$. After analyzing the simplified receiver circuit, the reflected components in the transmitter side can be computed as:

$$C_{ref} = (\frac{L_r}{L_t})(\frac{C_r}{k^2}), \tag{5.13}$$

$$R_{ref} = k^2(\frac{L_t}{L_r})R_{pt}. \tag{5.14}$$

The next step is to compute the total impedance which is seen from the transmitter. The total impedance Z_{tot} of the transmitter also equals to the combination of real part Z_{real} and the imaginary part Z_{ima} which is expressed as:

$$Z_{tot} = Z_{real} + jZ_{ima}. \tag{5.15}$$

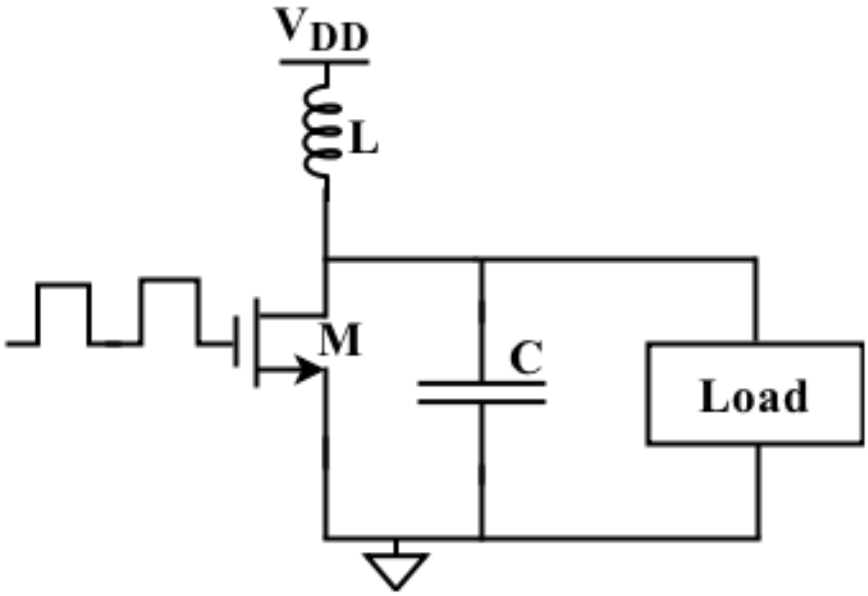

Figure 5.6 Circuit diagram of a basic class E power amplifier.

Then, the real and imaginary parts of Z_{tot} are computed.

$$Z_{real}(\omega, k) = R_t + \frac{\omega^2 k^4 L_t^2 R_{ref}}{(R_{ref} - \omega^2 R_{ref} k^2 L_t^2 C_{ref})^2 + (\omega k^2 L_t)^2}, \tag{5.16}$$

$$\begin{aligned} Z_{ima}(\omega, k) =& \frac{\omega k^2 L_t R_{ref}(R_{ref} - \omega^2 R_{ref} k^2 L_t C_{ref})}{(R_{ref} - \omega^2 R_{ref} k^2 L_t C_{ref})^2 + (\omega k^2 L_t)^2} \\ &+ \omega((1 - k^2)L_t + C_t). \end{aligned} \tag{5.17}$$

The electrical components in these equations (5.13), (5.15), (5.16) and (5.17) are fixed. The impedance value can be changed according to the angular frequency ω and the coupling factor k. Under the condition of misalignment, these impedance values are impacted due to the change in the coupling factor. To understand the misalignment in wireless power transfer system, a class E power amplifier needs to be studied. In the next section, the analysis of class E power amplifier is performed [42].

5.1.3 Class E power amplifier

To drive the primary coil, a DC to AC converter is utilized. Among different kinds of power amplifier that meet the basic requirement of the WPT system (class F, class J and class E), class E power amplifier is selected as the main driver circuit of the primary coil because it offers the largest power transfer efficiency [43]. By achieving the zero-voltage switching (ZVS) and zero-voltage derivative switching (ZVDS) conditions, traditionally, the power efficiency of the class E amplifier is 100 %.

The basic circuit structure of class E power amplifier is shown in Fig. 5.6. The ON and OFF states of the transistor are controlled by a pulse signal. When the transistor is turned on, it will short the shunt capacitor C. When the transistor is turned off, all of the power will go through the load of power amplifier. If the working condition of the class E power amplifier is ZVS and ZVDS, there is no power loss on the transistor. All of the power which comes from the power supply is going to deliver to the load. In biomedical implants, it is highly desirable to get the maximum power transfer efficiency. Therefore, the class E power amplifier is selected as the driver.

By implementing the class E power amplifier in the wireless power transfer system, a detailed analysis needs to be performed to generate the compensation results. Before going into the detail, some assumptions are made:

1) The MOSFET transistor has no turn on and turn off resistance.

2) The duty cycle of the pulse signal generator is set to 50 %.

3) The quality factor of the load is high enough, such that the transmitter current can be seen as a pure sine waveform:

$$i_t(\omega t) = I_m sin(\omega t + \phi). \tag{5.18}$$

If the turn on and off resistance of the transistor are included, then some power is lost

due to the MOSFET transistor.

By applying KCL at the drain node of MOSFET, the relationship of the current i_{L_D}, i_{DS}, i_C, i_t is established.

$$i_{L_D}(\omega t) = i_{DS}(\omega t) + i_C(\omega t) + i_t(\omega t). \tag{5.19}$$

Here, i_{L_D} is the current from the power supply. i_{DS} is the drain current of the MOSFET, i_C represents the current passing through the shunt capacitor C_{shunt} and i_t is the transmitter current which goes through the primary coil. The KVL is also applied at the drain node. Voltage related equation is also derived as:

$$V_{DD} - v_{DS}(\omega t) = v_{L_D} = \omega L_D \frac{di_{L_D}(\omega t)}{d\omega t}. \tag{5.20}$$

Here, V_{DD} is the supply voltage, v_{DS} is the drain voltage across the transistor and v_{L_D} is the voltage across the drain inductor.

To derive the analytical expressions for the transient behavior of $v_{DS}(\omega t)$, two scenarios are considered depending on the region of operation of the MOSFET switch, .

i) When the MOSFET is completely on ($0 \leq \omega t < \pi$). In this case, the shunt capacitor is shorted. Therefore, the drain voltage of the MOSFET, $v_{DS}(\omega t)$, is 0, and the shunt capacitor current, $i_C(\omega t)$, also equals to 0. These two situations can be applied to (5.19) and (5.20), resulting in two new equations:

$$i_{L_D}(\omega t) = i_{DS}(\omega t) + i_t(\omega t) = i_{DS}(\omega t) + I_m sin(\omega t + \phi), \tag{5.21}$$

$$V_{DD} = v_{L_D} = \omega L_D \frac{di_{L_D}(\omega t)}{d\omega t}. \tag{5.22}$$

Using (5.22), the drain inductor current i_{L_D} can be derived:

$$i_{L_D}(\omega t) = \frac{1}{\omega L_D} \int_0^{\omega t} V_{DD} d\omega t + i_{L_D}(0) = (\frac{V_{DD}}{\omega L_D})\omega t + i_{L_D}(0). \tag{5.23}$$

When ωt=0, the initial state of drain inductor current is obtained:

$$i_{L_D}(0) = I_m sin(\phi). \tag{5.24}$$

Accordingly, (5.23) can be rewritten as:

$$i_{L_D}(\omega t) = (\frac{V_{DD}}{\omega L_D})\omega t + I_m sin(\phi). \tag{5.25}$$

ii) When the MOSFET is completely off ($\pi \leq \omega t < 2\pi$). In this case, the MOSFET is modeled as an open circuit. Therefore,

$$i_{DS}(\omega t) = 0, \tag{5.26}$$

$$v_{DS}(\omega t) = v_C(\omega t). \tag{5.27}$$

Under these situations, (5.19) and (5.20) can be derived as:

$$i_{L_D}(\omega t) = i_C(\omega t) + i_t(\omega t) = i_C(\omega t) + I_m sin(\omega t + \phi), \tag{5.28}$$

$$V_{DD} - v_C(\omega t) = v_{L_D} = \omega L_D \frac{di_{L_D}(\omega t)}{d\omega t}. \tag{5.29}$$

The current and voltage of the shunt capacitor, C_{shunt} should satisfy

$$i_C(\omega t) = \omega C_{shunt} \frac{dv_C(\omega t)}{d\omega t}. \tag{5.30}$$

$v_c(\omega t)$ in (5.30) can be replaced by using (5.29). Therefore, the equation for $i_C(\omega t)$ can be expressed as:

$$i_C(\omega t) = \omega^2 C_{shunt} L_D \frac{d^2 i_{L_D}(\omega t)}{d\omega t^2}. \tag{5.31}$$

Using KCL which is expressed in (5.19), the inductor current can be derived :

$$i_{L_D}(\omega t) = \omega^2 C_{shunt} L_D \frac{d^2 i_{L_D}(\omega t)}{d\omega t^2} - I_m sin(\omega t + \phi). \tag{5.32}$$

(5.32) is a linear second order differential equation with respect to $i_{L_D}(\omega t)$. It can be solved as:

$$\frac{i_{L_D}(\omega t)}{I_m} = Asin(\alpha\omega t) + Bcos(\alpha\omega t) + \frac{\alpha^2 sin(\omega t + \phi)}{\alpha^2 - 1}, \tag{5.33}$$

where

$$\alpha = \frac{1}{\omega\sqrt{L_D C_{shunt}}}. \tag{5.34}$$

Here, A and B are the two factors which are determined by the boundary conditions of (5.32).

During the transition of the transistor from the ON to the OFF state, the inductor's current, i_{L_D}, and the voltage across the shunt capacitor, V_C, must remain continuous. Therefore, the boundary conditions for i_{L_D} and its derivative, i'_{L_D}, at $\omega t{=}\pi$ can be written as:

$$i_{L_D}(\pi^+) = i_{L_D}(\pi^-) = \frac{V_{DD}\pi}{\omega L_D} + I_m sin(\phi), \tag{5.35}$$

$$i'_{L_D}(\pi^-) = i'_{L_D}(\pi^+) = \frac{V_{DD}}{\omega L_D} \tag{5.36}$$

These boundary conditions can be applied in (5.33) to solve the factors A and B. Then we obtain:

$$\frac{i_{L_D}}{I_m}(\pi^+) = \frac{\pi}{\beta} + sin(\phi), \tag{5.37}$$

and

$$\frac{i'_{L_D}}{I_m}(\pi^+) = \frac{1}{\beta}, \tag{5.38}$$

where β is defined as

$$\beta = \frac{I_m L_D \omega}{V_{DD}}. \tag{5.39}$$

As a result, A and B are derived as:

$$A = \frac{1}{\alpha^2-1}[\alpha cos(\alpha\pi)cos(\phi)+(2\alpha^2{-}1)sin(\alpha\pi)sin(\phi)]+\frac{\pi}{\beta}sin(\alpha\pi)+\frac{1}{\alpha\beta}cos(\alpha\pi), \tag{5.40}$$

$$B = \frac{1}{\alpha^2-1}[-\alpha sin(\alpha\pi)cos(\phi) + (2\alpha^2-1)cos(\alpha\pi)sin(\phi)] + \frac{\pi}{\beta}cos(\alpha\pi) - \frac{1}{\alpha\beta}sin(\alpha\pi). \tag{5.41}$$

The voltage across the source and drain of the transistor during the OFF state can then be obtained from (5.20) by using i_{L_D} in (5.33),

$$\begin{aligned} v_{DS}(\omega t) =& V_{DD} - \beta V_{DD}[\alpha A cos(\alpha\omega t) - \alpha B sin(\alpha\omega t)+ \\ & \frac{\alpha^2 cos(\omega t+\phi)}{\alpha^2-1}]. \qquad\qquad (\pi \le \omega t < 2\pi) \end{aligned} \tag{5.42}$$

The expression of $v_{DS}(\omega t)$ during the full period can be derived based on the above analysis. During $0 \leq \omega t < \pi$, the MOSFET is turned on without any resistance indicating that $v_{DS}(\omega t)$ equals to 0. In the second half, $\pi \leq \omega t < 2\pi$, $v_{DS}(\omega t)$ follows expression described in (5.42).

To maintain an optimum working condition of class E power amplifier, the ZVS and ZVDS conditions need to be satisfied. The two conditions can be expressed by using equations:

$$v_{DS}(2\pi) = v_{DS}^{'}(2\pi) = 0, \tag{5.43}$$

where $v_{DS}^{'}$ is the derivation of v_{DS}. The conditions should be applied to (5.42), then two new equations are derived:

$$V_{DD} - \beta V_{DD}[\alpha A cos(\alpha 2\pi) - \alpha B sin(\alpha 2\pi) + \frac{\alpha^2}{\alpha^2 - 1}(cos\phi)] = 0, \tag{5.44}$$

and

$$\beta V_{DD}[\alpha A sin(\alpha 2\pi) + \alpha B cos(\alpha 2\pi) + \frac{\alpha^2}{\alpha^2 - 1}(sin\phi)] = 0. \tag{5.45}$$

From these equations, β and ϕ can be derived as functions of α to satisfy both conditions.

$$\beta = f(\alpha), \tag{5.46}$$

$$\phi = u(\alpha). \tag{5.47}$$

Based on the assumptions stated earlier in the section, there are no losses on the transistor of class E power amplifier. Therefore, the power taken from the power supply is received by Z_{real} which is the real part of the transmitter resistance illustrated in the reflected resistance section and can be expressed as:

$$V_{DD} I_o = \frac{1}{2} I_m^2 Z_{real}(\omega, k). \tag{5.48}$$

where I_o is the DC supply current and k is the coupling factor. The current I_o is derived as the average of the total current going through the supply voltage during the whole

period,

$$I_o = \frac{1}{2\pi}\int_0^{2\pi} i_{L_D}(\omega t)d\omega t. \tag{5.49}$$

By simplifying the right side of (5.49), I_o can be obtained:

$$I_o = \frac{I_m}{2}(\frac{\pi}{2\beta} - \frac{2}{\pi}cos(\phi) + sin(\phi)). \tag{5.50}$$

Replacing (5.34), (5.39) and (5.50) in (5.49) one can obtain:

$$\alpha^2\beta Z_{real}(\omega, k)C_{shunt} - (\frac{\pi}{2\beta} - \frac{2}{\pi}cos(\phi) + sin(\phi)) = 0. \tag{5.51}$$

To satisfy the ZVS and ZVDS conditions, parameters β and ϕ can be derived as functions of α. By replacing (5.46), (5.47) in (5.51) and knowing the α depends on the ω, it can be seen that variations in ω or k could impact the equality in (5.51).

All of the above equations concerning the class E power amplifier are derived under the optimum working conditions. In the case of misalignment, the coupling factor is going to be changed. This variation will alter the working condition of the class E power amplifier, meaning (5.51) cannot hold its equality. Additionally, based on the circuit analysis, the power delivered to the load is also changed. Thus, an approach needs to be developed to solve these problems in WPT system under coils misalignment. The proposed compensation approach is introduced in the next section.

5.2 Proposed Compensation Concept

5.2.1 Illustration of Misalignment Compensation Concept

The main goal of the proposed compensation concept is to ensure that the class E amplifier works at ZVS and ZVDS operating conditions, and $V_{load_{peak}}$, as defined in (5.10), remains constant. These key parameters could be easily changed because of the coupling factor due to the misalignment.

To maintain the optimum operational condition of the class E amplifier, (5.44), (5.45) and (5.48) need to be satisfied. (5.51) is the combination of these equations. If the coupling factor is altered due to the misalignment, (5.51) cannot hold its equality. It means that the operation of class E amplifier is not optimum and hence a new α needs to be derived. To hold the equality of (5.44) and (5.45), β and ϕ can be expressed using α. The expressions of β and α are applied in (5.51). According to (5.34), α depends on the electrical components of the circuits and the angular frequency ω. By keeping ω and drain inductor L_D constant, the parameter C_{shunt} can be altered at the transmitter side to obtain the required new α, corresponding to the new β and ϕ to ensure that the class E power amplifier works at its optimum operating condition.

In this situation, the optimum operating condition of class E power amplifier is achieved. But the power delivered to the load could still vary. According to (5.39), the new value of β can force I_m to change, if V_{DD}, ω and L_D are kept constant. Therefore, in (5.10), the coupling factor k and the peak transmitter current I_m both change, resulting in a variation in the peak voltage at the load, $V_{load_{peak}}$. However, if the change in I_m can be controlled, it will compensate for the variation in k, generating a stable load peak voltage. This can be achieved by changing the supply voltage V_{DD} in the transmitter and fixing the drain inductor. In (5.39), once β and L_D are fixed, accordingly the I_m can be changed to a desired value for compensation by altering the supply voltage to a specific number.

To summarize, if k changes due to misalignment, altering the shunt capacitor and the supply voltage at the transmitter side could be a potential solution to ensure the WPT system continues to deliver a stable power to the load even in the presence of misalignment.

5.2.2 Simulation Results

To validate the proposed concept for compensation concept, simulations were performed using MATLAB (based on the analytical expression) and Cadence (based on circuit simulation). The component values used for circuit simulation were taken from [40]. The duty cycle of the driver signal applied to the gate of the transistor was set to 50%.

The coupling factor, k, and the load peak voltage value in the absence of misalignment, were set to 0.3 and 3.5 V, respectively. To model different misalignment scenarios, the value of the coupling factor, k, was manually changed. For each k, the shunt capacitor and the supply voltage required for achieving an optimum working condition of the class E amplifier and to maintain the peak voltage value at 3.5 V were obtained analytically using MATLAB. The values of these design parameters can be obtained by computing the equations which are shown in class E power amplifier analysis section.

To get simulation results, the circuit schematic shown in Fig. 5.1 is built in Cadence. The coupling factor of the two coupled coils in this circuit is changed, and the shunt capacitor is also changed, accordingly. By analyzing the waveform of v_{DS}, the proper value of the shunt capacitor C_{shunt} is recorded to deliver a ZVS and ZVDS drain voltage waveform. After that, the supply voltage V_{DD} is altered to get the stable load peak voltage by seeing the load voltage V_{load} waveform. The proper supply voltage values are also recorded.

Fig. 5.7 and Fig. 5.8 show required supply voltage values and shunt capacitor values for compensating the negative effect of the misalignment, obtained analytically and through simulation, respectively.

Transient simulation is also performed to validate the proposed concept. The transient simulation shows the load voltage and drain voltage, respectively. The simulation is

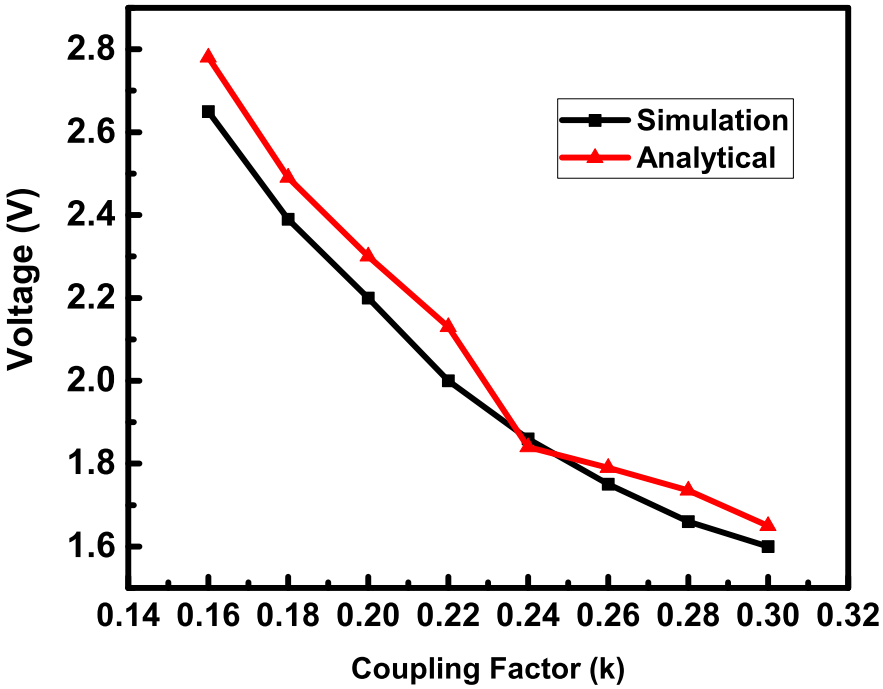

Figure 5.7 Calculated and simulated supply voltage values in WPT transmitter to achieve compensation in presence of misalignment.

performed under three different scenarios:

a). The ideal case is no misalignment, under this scenario, k=0.3.

b). k is set to 0.28 due to the presence of misalignment. There is no compensation method applied in this situaition.

c). k is set to 0.28 due to the coil misalignment, however, the proposed compensation concept is applied. It means that the shunt capacitor and the supply voltage have been adjusted to keep the class E amplifier to work optimally to maintain the peak voltage value to be the same as the case when there was no misalignment. The simulation results of the different scenarios are shown in Fig. 5.9, Fig. 5.10 and Fig. 5.11 respectively.

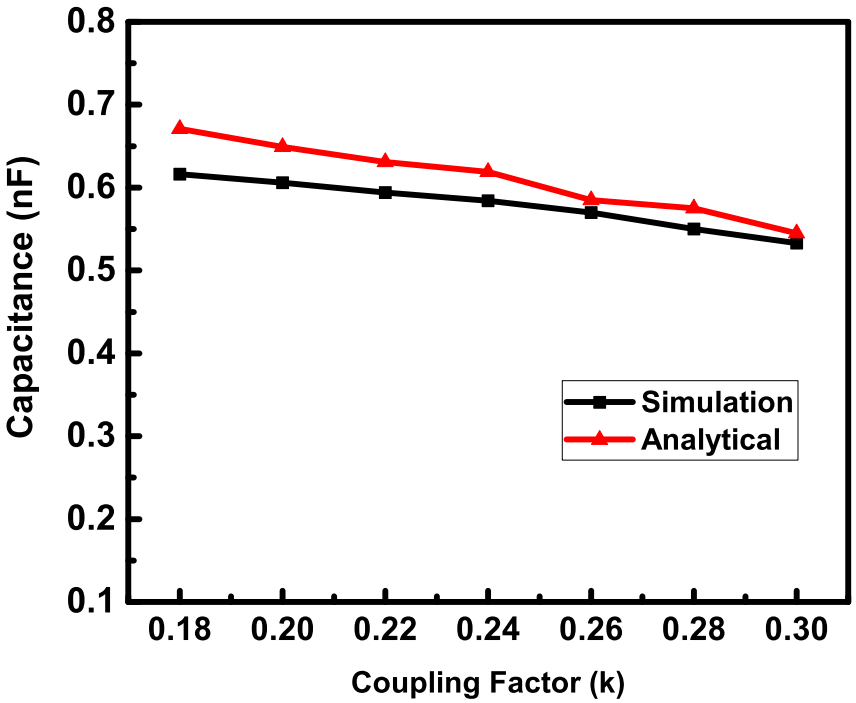

Figure 5.8 Calculated and simulated shunt capacitor values in WPT transmitter to achieve compensation in presence of misalignment.

The ideal situation is shown in Fig. 5.9, it illustrates the class E power amplifier is working at its optimum situation. Under the condition of misalignment, which is simulated by reducing the coupling factor to 0.28, Fig. 5.10 shows a non-optimum operating condition for class E power amplifier where the load peak voltage is also accordingly reduced. By tuning the shunt capacitor and supply voltage, the working condition of class E power amplifier is restored and the load peak voltage reaches to the original value. These results verify that our proposed compensation concept can mitigate the negative effects of coils misalignment.

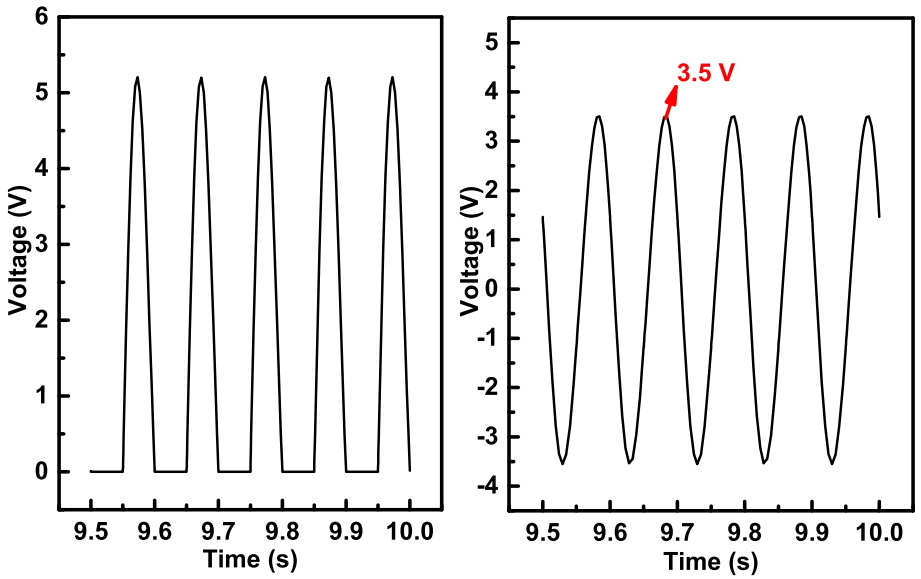

Figure 5.9 Simulated waveforms on the drivers drain voltage, V_{ds}, and on the loads peak voltage under optimum operation condition at k=0.3.

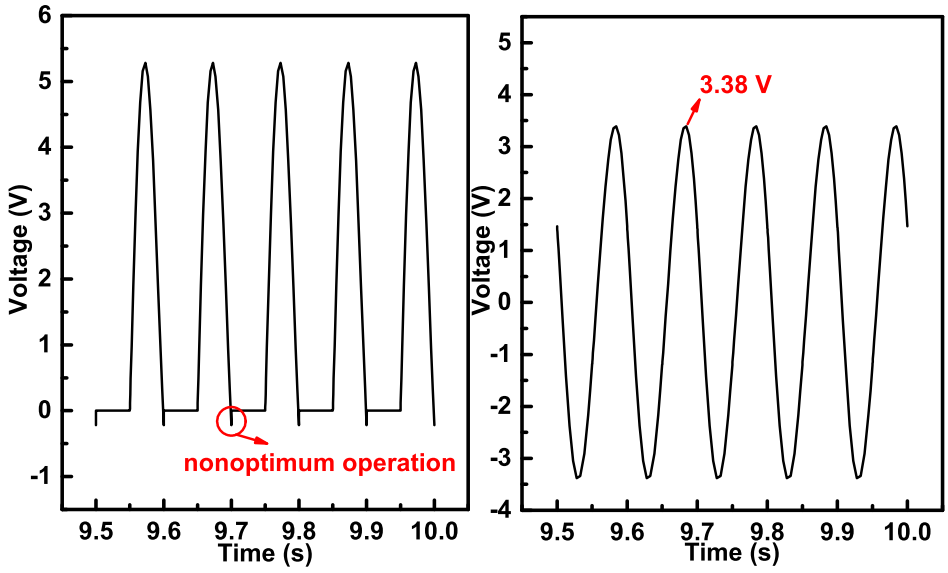

Figure 5.10 Simulated waveforms on the drivers drain voltage, V_{ds}, and on the loads peak voltage under the presence of misalignment at k=0.28, no compensation.

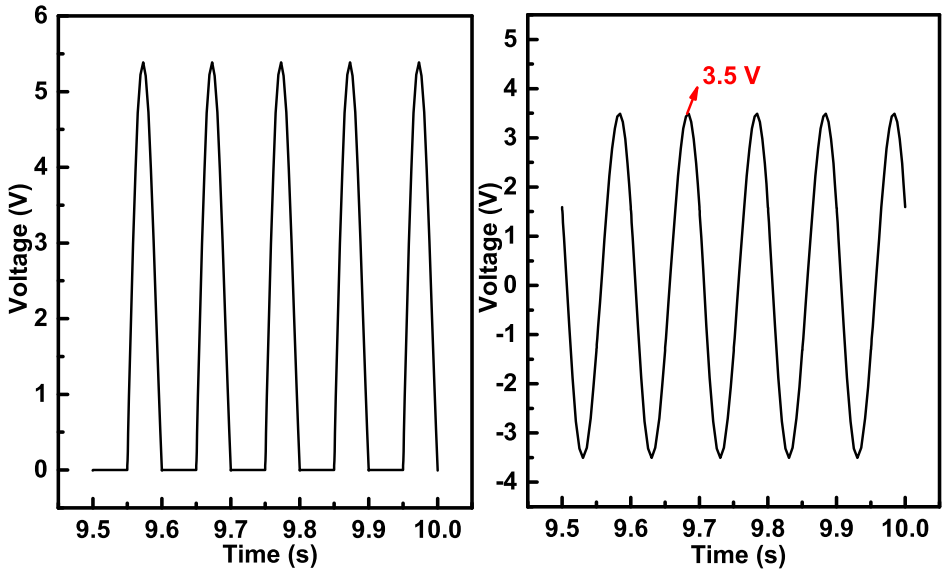

Figure 5.11 Simulated waveforms on the drivers drain voltage, V_{ds}, and on the loads peak voltage under the presence of misalignment at k=0.28, with applying compensation.

5.2.3 Advantages of the proposed misalignment compensation design

There are three main merits of this proposed method.

First, several proposed techniques use tuning of the working frequency for compensation [3] [4]. However, this method has its disadvantage. According to [5], the disadvantage is that changing the working frequency is going to alter the power transfer efficiency of the coupled coils. It is undesirable to change the power transfer efficiency of the coupled coils while solving the misalignment problems. Therefore, to overcome the changing power transfer efficiency disadvantage, in our proposed method the working frequency remains the same to ensure a stable power transfer efficiency.

Second, the misalignment will not only change the power delivered to the load, but the working condition of the class E power amplifier is also altered. Most of previous

design did not address this issue. In our design method, the class E power amplifier can restore its optimum working condition even under the misalignment situations. Also the power delivered to the load can be maintained a constant.

Third, to realize the previous proposed techniques, some additional circuitry is required. This will increase the design difficulty of the system. For example, in [3], the drain inductor was changed to address for misalignment compensation. To change the inductor, an extra component was added in the transmitter increasing the complexity of the system. In our proposed method, by designing an integrated system, the shunt capacitor can be tuned by using a varactor, for example. There is no need for extra components hence reducing the design difficulty.

5.3 Conclusion

In this chapter, a compensation concept for mitigating the negative effects of coil misalignment in wireless power transfer links used in biomedical implants was presented. The circuit theory for the operation of wireless power transfer system was discussed in detail. The receiver circuit was analyzed for deriving the expression of the peak voltage. Then, the reflected impedance theory was used for obtaining the operating condition of the class E power amplifier. Based on the derived equations, a compensation method, by altering the shunt capacitor and supply voltage, was proposed. Simulation results based on the proposed compensation concept were also presented verifying the validation of proposed method.

Chapter 6

Conclusions

Wireless power transfer (WPT) technique finds applications in variety of systems, especially in biomedical implants. For biomedical implants, delivering a constant power is highly desired and the power transfer efficiency should be maximized [42]. One of the issue which adversely affects the power transmission is the misalignment between the coils forming [30]. To mitigate this effect, a design compensation concept, which can achieve a stable load power delivery and maintain the driver circuit working in its optimum condition without changing the power transfer efficiency of the inductive link was proposed.

The contributions of this thesis are listed as follows:

1 . An overview of wireless power transfer technique was presented. Based on the distance d of wireless power transfer and the power transfer wavelength λ, three categories were demonstrated: near field ($d < \lambda/2\pi$), mid field ($\lambda/2\pi < d < \lambda/\pi$) and far field ($d > \lambda/\pi$). If the power needs transferring via a large distance, the microwave or photo-electricity techniques are adopted. To transfer power in centimeters range, such as in biomedical implants, the magnetic coupling method in generally selected. If the power transfer distance is in mid field range, the combination of inductive and radiative models is utilized.

2 . Different structures for the magnetic coupling, classified as resonant coupling

and inductive coupling in biomedical implants, were introduced [5]. The resonance based wireless power transfer structures have been used because it can achieve higher power transfer efficiency than inductive coupling [5]. Based on the number of the coils, two-coil, three-coil and four-coil based resonant wireless power transfer systems were demonstrated. The models of these structures were mathematically analyzed using math equations. The design parameters, such as the power transfer efficiency, were computed.

3 . The issue of the coil misalignment was reviewed. Two different scenarios of the misalignment, the angular and position displacement, were presented. The mutual inductance of the misalignment coils was computed. It was shown that once the misalignment happens, the mutual inductance and the coupling factor k are highly impacted.

4 . The prior work regarding the misalignment compensation in wireless power transfer was reviewed. First, it was proposed that tuning the operational frequency is a method to compensate the negative effect induced by the misalignment of primary and secondary coils. Additionally, the power supply in the transmitter side has been proved to be another method to do the compensation. To realize the method of altering power supply, radio frequency (RF) transceiver has been built in the receiver and transmitter for transferring data. According to these transferred data, the proper amount of supply voltage for tuning can be obtained. Finally, the off-the-shelf components are used to built the wireless power transfer system. By programming these products, the misalignment issues can be solved.

5 . The presented misalignment compensation design concept was presented. The receiver circuit was analyzed for computing the power received by the load. The reflected impedance theory and the driver circuit were discussed. Based on these

theory, it was shown that by tuning the shunt capacitor and the supply voltage, the misalignment can be compensated, achieving the optimum working condition of the class E power amplifier and maintaining a constant power delivery to the load. Simulation results were performed to verify valitity of the proposed the concept.

Bibliography

[1] Mehdi Kiani and Maysam Ghovanloo. Near-field wireless power and data transmission to implantable neuroprosthetic devices. In *Neural Computation, Neural Devices, and Neural Prosthesis*, pages 189–215. Springer, 2014.

[2] Shawon Senjuti. Design and optimization of efficient wireless power transfer links for implantable biotelemetry systems (thesis format: Monograph), 2013.

[3] Samer Aldhaher, PC-K Luk, and James F Whidborne. Electronic tuning of misaligned coils in wireless power transfer systems. *Power Electronics, IEEE Transactions on*, 29(11):5975–5982, 2014.

[4] Philip R Troyk and Martin AK Schwan. Closed-loop class e transcutaneous power and data link for microimplants. *Biomedical Engineering, IEEE Transactions on*, 39(6):589–599, 1992.

[5] Rajiv Jay and Samuel Palermo. Resonant coupling analysis for a two-coil wireless power transfer system. In *Circuits and Systems Conference (DCAS), 2014 IEEE Dallas*, pages 1–4, 2014.

[6] Nattapon Chaimanonart, Mark D Zimmerman, and Darrin J Young. Adaptive rf power control for wireless implantable bio-sensing network to monitor untethered laboratory animal real-time biological signals. In *Sensors, 2008 IEEE*, pages 1241–1244, 2008.

[7] Mehdi Kiani and Maysam Ghovanloo. An RFID-based closed-loop wireless power

transmission system for biomedical applications. *Circuits and Systems II: Express Briefs, IEEE Transactions on*, 57(4):260–264, 2010.

[8] Richard S Sanders and Michel T Lee. Implantable pacemakers. *Proceedings of the IEEE*, 84(3):480–486, 1996.

[9] Francis A Spelman. The past, present, and future of cochlear prostheses. *Engineering in Medicine and Biology Magazine, IEEE*, 18(3):27–33, 1999.

[10] Seung Bae Lee, Byunghun Lee, Benoit Gosselin, and Maysam Ghovanloo. A dual slope charge sampling analog front-end for a wireless neural recording system. In *Engineering in Medicine and Biology Society (EMBC), 2014 36th Annual International Conference of the IEEE*, pages 3134–3137, 2014.

[11] R-F Xue, K-W Cheng, and Minkyu Je. High-efficiency wireless power transfer for biomedical implants by optimal resonant load transformation. *Circuits and Systems I: Regular Papers, IEEE Transactions on*, 60(4):867–874, 2013.

[12] Zhen Ning Low, Raul Andres Chinga, Ryan Tseng, and Jenshan Lin. Design and test of a high-power high-efficiency loosely coupled planar wireless power transfer system. *Industrial Electronics, IEEE Transactions on*, 56(5):1801–1812, 2009.

[13] Anil Kumar RamRakhyani, Shahriar Mirabbasi, and Mu Chiao. Design and optimization of resonance-based efficient wireless power delivery systems for biomedical implants. *Biomedical Circuits and Systems, IEEE Transactions on*, 5(1):48–63, 2011.

[14] Michael P Theodoridis. Effective capacitive power transfer. *Power Electronics, IEEE Transactions on*, 27(12):4906–4913, 2012.

[15] Amir M Sodagar and Parviz Amiri. Capacitive coupling for power and data telemetry to implantable biomedical microsystems. In *Neural Engineering, 2009. NER'09.*

4th International IEEE/EMBS Conference on, pages 411–414, 2009.

[16] H Zheng, K Tnay, N Alami, and AP Hu. Contactless power couplers for respiratory devices. In *Mechatronics and Embedded Systems and Applications (MESA), 2010 IEEE/ASME International Conference on*, pages 155–160, 2010.

[17] Aiguo Patrick Hu, Chao Liu, and Hao Leo Li. A novel contactless battery charging system for soccer playing robot. In *Mechatronics and Machine Vision in Practice, 2008. M2VIP 2008. 15th International Conference on*, pages 646–650. IEEE, 2008.

[18] Mitchell Kline, Igor Izyumin, Bernhard Boser, and Seth Sanders. Capacitive power transfer for contactless charging. In *Applied Power Electronics Conference and Exposition (APEC), 2011 Twenty-Sixth Annual IEEE*, pages 1398–1404, 2011.

[19] Byung Woo Yoon. Power delivery circuit for scalable claytronics. *MSc Report, Carnegie Mellon University, Department of Electrical and Computer Engineering*, 2007.

[20] Farzad Asgarian and Amir M Sodagar. *Wireless Telemetry for Implantable Biomedical Microsystems*. INTECH Open Access Publisher, 2011.

[21] Mustafa Emre Karagozler, Jason D Campbell, Gary K Fedder, Seth Copen Goldstein, Michael Philetus Weller, and Byung Woo Yoon. Electrostatic latching for inter-module adhesion, power transfer, and communication in modular robots. In *Intelligent Robots and Systems, 2007. IROS 2007. IEEE/RSJ International Conference on*, pages 2779–2786, 2007.

[22] Bert Lenaerts and Robert Puers. *Omnidirectional inductive powering for biomedical implants*. Springer, 2009.

[23] Yiming Zhang, Zhengming Zhao, and Kainan Chen. Frequency decrease analysis

of resonant wireless power transfer. *Power Electronics, IEEE Transactions on*, 29 (3):1058–1063, 2014.

[24] Nikola Tesla. The transmission of electrical energy without wires as a means for furthering peace. *Electrical World and Engineer. Jan*, 7:21, 1905.

[25] William C Brown. The technology and application of free-space power transmission by microwave beam. *Proceedings of the IEEE*, 62(1):11–25, 1974.

[26] David Smith. Wireless power spells end for cables. *The Observer (London)*, 2009.

[27] John S Ho, Sanghoek Kim, and Ada SY Poon. Midfield wireless powering for implantable systems. *Proceedings of the IEEE*, 101(6):1369–1378, 2013.

[28] Ada SY Poon, Stephen O'Driscoll, and Teresa H Meng. Optimal frequency for wireless power transmission into dispersive tissue. *Antennas and Propagation, IEEE Transactions on*, 58(5):1739–1750, 2010.

[29] Mehdi Kiani, Uei-Ming Jow, and Maysam Ghovanloo. Design and optimization of a 3-coil inductive link for efficient wireless power transmission. *Biomedical Circuits and Systems, IEEE Transactions on*, 5(6):579–591, 2011.

[30] Kyriaki Fotopoulou and Brian W Flynn. Wireless power transfer in loosely coupled links: Coil misalignment model. *Magnetics, IEEE Transactions on*, 47(2):416–430, 2011.

[31] Frederick Warren Grover. *Inductance calculations: working formulas and tables*. Courier Corporation, 1946.

[32] Chester Snow. *Formulas for computing capacitance and inductance*, volume 544. US Govt. Print. Off., 1954.

[33] FC Flack, ED James, and DM Schlapp. Mutual inductance of air-cored coils: Effect

on design of radio-frequency coupled implants. *Medical and biological engineering*, 9(2):79–85, 1971.

[34] Erwin S Hochmair. System optimization for improved accuracy in transcutaneous signal and power transmission. *Biomedical Engineering, IEEE Transactions on*, (2):177–186, 1984.

[35] Slobodan I Babic and Cevdet Akyel. Calculating mutual inductance between circular coils with inclined axes in air. *Magnetics, IEEE Transactions on*, 44(7): 1743–1750, 2008.

[36] Milton Abramowitz, Irene A Stegun, et al. *Handbook of mathematical functions*, volume 1. Dover New York, 1972.

[37] Izrael Solomonovich Gradshtejn and Iosif Moiseevich Ryzhik. *Table of integrals, series and products*. Academic Press, 1965.

[38] Guoxing Wang, Wentai Liu, Mohanasankar Sivaprakasam, and Gurhan Alper Kendir. Design and analysis of an adaptive transcutaneous power telemetry for biomedical implants. *Circuits and Systems I: Regular Papers, IEEE Transactions on*, 52(10):2109–2117, 2005.

[39] P Si, AP Hu, JW Hsu, M Chiang, Y Wang, S Malpas, and D Budgett. Wireless power supply for implantable biomedical device based on primary input voltage regulation. In *Industrial Electronics and Applications, 2007. ICIEA 2007. 2nd IEEE Conference on*, pages 235–239. IEEE, 2007.

[40] Gurhan Alper Kendir, Wentai Liu, Guoxing Wang, Mohanasankar Sivaprakasam, Rizwan Bashirullah, Mark S Humayun, and James D Weiland. An optimal design methodology for inductive power link with class-e amplifier. *Circuits and Systems I: Regular Papers, IEEE Transactions on*, 52(5):857–866, 2005.

[41] Mehdi Kiani and Maysam Ghovanloo. The circuit theory behind coupled-mode magnetic resonance-based wireless power transmission. *Circuits and Systems I: Regular Papers, IEEE Transactions on*, 59(9):2065–2074, 2012.

[42] Fanpeng Kong, Yi Huang, and Laleh Najafizadeh. A coil misalignment compensation concept for wireless power transfer links in biomedical implants. In *Wireless Power Transfer Conference (WPTC), 2015 IEEE*, pages 1–4, 2015.

[43] Seunghoon Jee, Junghwan Moon, Jungjoon Kim, Junghwan Son, and Bumman Kim. Switching behavior of class-e power amplifier and its operation above maximum frequency. *Microwave Theory and Techniques, IEEE Transactions on*, 60(1): 89–98, 2012.